Spring 2018

Fabrication and characterization of advanced materials using laser metal deposition from elemental powder mixture

Xueyang Chen

Department: Mechanical and Aerospace Engineering

FABRICATION AND CHARACTERIZATION OF ADVANCED MATERIALS USING LASER METAL DEPOSITION FROM ELEMENTAL POWDER MIXTURE

by

XUEYANG CHEN

A DISSERTATION

Presented to the Faculty of the Graduate School of the

MISSOURI UNIVERSITY OF SCIENCE AND TECHNOLOGY

In Partial Fulfillment of the Requirements for the Degree

DOCTOR OF PHILOSOPHY

in

MECHANICAL ENGINEERING

2018

Approved
Dr. Frank Liou, Advisor
Dr. Ashok Midha
Dr. K. Chandrashekhara
Dr. Heng Pan
Dr. Xiaoming He

PUBLICATION DISSERTATION OPTION

This dissertation consists of the following three articles that have been published or submitted for publication as follows:

Paper I, pages 6-21 have been published in Journal of Mechanics Engineering and Automation.

Paper II, pages 22-47 are intended for submission to JOM.

Paper III, pages 48-74 have been published in Coatings.

Paper IV, pages 75-93 have been accepted for publication for 2017 Annual International Solid Freeform Fabrication Symposium and are intended for submission to Rapid Prototyping Journal.

All of them have been prepared in the Missouri University of Science and Technology dissertation format.

ABSTRACT

Over the past decades of years, a great deal of money has been spent to machine large and complex parts from high-performance metals (i.e., titanium components for aerospace applications), so users attempt to circumvent the high cost of materials. Laser metal deposition (LMD) is an additive manufacturing technique capable of fabricating complicated structures with superior properties. This dissertation aims to improve the applications of LMD technique for manufacturing metallic components by using various elemental powder mixture according to the following three categories of research topics. The first research topic is to investigate and develop a cost-effective possibility by using elemental powder mixture for metallic components fabrication. Based on the studies of fabricating thin-wall Ti-6Al-4V using elemental powder mixture, comparative close particle number for Ti, Al and V powder could easily get industry qualified Ti-6Al-4V components. The particle number for each element in powder blends has been proved to be a key factor for composition control in the final deposit part. The second research topic focuses on the application improvements of elemental powder manufacturing. By fabricating $Al_xCoFeNiCu_{1-x}$ (x = 0.25, 0.5, 0.75) high entropy alloys from elemental powder based feedstocks, it enhances the usage of elemental powder to fabricate novel materials with complex compositions. The third research topic extends the applications of using elemental powder mixture to the broader area. A functionally gradient material (FGM) path is developed to successfully join titanium alloy with γ-TiAl. This dissertation leads to new knowledge for the effective fabrication of unique and complex metallic components. Moreover, the research results of the dissertation could benefit a wide range of industries.

ACKNOWLEDGMENTS

First and foremost, I would like to express my sincere gratitude to my advisor, Dr. Frank Liou, for his encouragement, insightful guidance, and support during my Ph.D. study at Missouri University of Science and Technology. His diligence and rigorous altitude to research and work will have a significant influence on my life. It has been a privilege and a great honor to have worked with him.

I would also like to extend my appreciation to all my dissertation committee members, Dr. Ashok Midha, Dr. K. Chandrashekhara, Dr. Heng Pan, and Dr. Xiaoming He. Without their guidance and valuable comments, it would have been impossible for me to complete my dissertation.

This dissertation was supported by the Laser Aided Manufacturing Processes (LAMP) Laboratory, and the Intelligent System Center of Missouri S&T, which are gratefully acknowledged.

I would like to express my deep thanks to my lab-mates and friends, Mr. Lei Yan, Mr. Sreekar Karnati, Mr. Yunlu Zhang, Mr. Jingwei Zhang, Mr. Xinchang Zhang, Mr. Wei Li, Mr. Todd Sparks, Mr. Connor L. Coward, Mr. Max Mulholland, Mr. Sriram Isanaka, Mr. Aeron Flood, Mr. Yitao Chen, Ms. Wenyuan Cui and Ms. Tan Pan, for their support during my study in Rolla.

Last but not the least, I wish to extend my special and sincere thanks to my parents, Mr. Fuan Chen and Ms. Saihua Li, and all my family members for their love and unwavering support.

TABLE OF CONTENTS

Page

LIST OF ILLUSTRATIONS

SECTION Page

PAPER III

PAPER IV

LIST OF TABLES

SECTION
1. INTRODUCTION

1.1. BACKGROUND

High-performance metal components are very costly, especially for large and complex parts (i.e., titanium components for aerospace applications). Typically, most of the advanced components are made of high-value materials such as titanium and nickel-based alloys. Nowadays, a variety of high quality and low-cost powders are available for manufacturing. It should lead to a reasonable growth of products manufactured by the powder-producing process. The benefits offered by the powder-producing techniques are well-known: reduce processing steps, no extensive secondary machining, low buy-to-use ratio, rapid manufacturing cycle, uniform properties in longitudinal and transverse directions, integral processing of composites, more energy efficient, etc [1]. Apart from these, a substantial advantage is that net shape or near net shape (NNS) parts can be made with little or no additional shaping in the process. Near net shape processing looks like the most appealing way to reduce high cost. From a chemistry standpoint, production of NNS parts is divided into parts produced using blended elemental (BE) powders and those produced using pre-alloyed (PA) powders. The elemental approach blends various suitable pure powders from the wide range of available powders to develop target properties. The PA approach involves the use of pre-alloyed powders, each particle is an alloy composed of the desired chemical composition. PA powders are usually used to produce large and complex parts, such as the impeller and arrestor hook support fitting. The elemental method is potentially more effective, flexible, and lower cost, also elemental powders are much easily processed than pre-alloyed powder. Compared with conventional techniques, laser

metal deposition (LMD) is an additive manufacturing technique capable of fabricating complicated structures with superior properties. The applications of this technique include coatings, rapid prototyping, tooling, repair, etc.

Even though LMD provides the good capability for various fabrication, some components could be unique and complex. For each individual component, the required composition and specific combination of mechanical properties are arbitrary, even the desired level of interstitials could be different. Even in one component, the geometry and area variation may exist because of different required functions. Meanwhile, high-value components are fabricated with expensive materials and more labor. Although compatible and affordable powders could be selected and blended to achieve desired components, many kinds of new powders are still under development. These new powders will not be available for some time until they establish the cost and characteristics [2]. It provides an opportunity to process components of equivalent or superior properties with a competitive cost. Currently, more and more metallic components could be fabricated by powder-producing method easily, especially in aerospace and automobile areas. The uniqueness of each component brings challenges to control the manufacturing processes, such as change the composition, control the energy density for different parts, produce new material area, etc. The dissertation develops production method to fabricate desired products using elemental powder mixture by LMD method with low cost, high accuracy, and good capability.

1.2. RESEARCH OBJECTIVES

The main objective of this dissertation is to investigate the approaches to fabricate and analyze different metal components using elemental powder mixture by LMD technique. Three topics are researched to describe and support the general method.

The objective of the research topic one is to fabricate thin-wall Ti-6Al-4V using the powder mixture of Ti-6wt.% Al-4wt.% V by LMD method. The main challenging problem in the deposition process is to confirm to get target material with the original weight percentage ratio. By understanding the size distribution and characteristics of powder particles, observations and any findings in deposits could potentially be correlated with these factors such as particle shape or size. Two hypothesis will be proposed to study the influence of particle acceleration and number of particles for each elemental powder on the as-built parts. Based on this analysis, the strategy can be identified to obtain industry qualified metallic components with elemental powder mixture by LMD technique.

Research topic two addresses the problem of how to improve the usage of elemental powder mixture when fabricating some new types of novel metallic components with complex composition. Take high entropy alloy as an example, $AlxCoFeNiCu1{-}x$ ($x = 0.25$, 0.5, 0.75) high entropy alloys have been successfully fabricated by the LMD technique using blended Al-Co-Fe-Ni-Cu elemental powder as the feedstock. The method is flexible for fabrication and development of the novel material system that exhibits more superior properties than traditional alloys [3]. Moreover, this method provides the feasibility to develop unique materials using elemental powder mixture with comparable low cost.

The third research topic is to develop a functionally graded material (FGM) path to successfully join titanium alloy with γ-TiAl using Ti-48Al-2Cr-2Nb and Ti powder via the

LMD process. Because there is a great difference in the thermal expansion coefficient between Ti and γ-TiAl, it will result in cracks during cooling process after deposition due to the high residual thermal stresses between layers. Thus it is necessary to develop a gradient path to deposit crack-free Ti/γ-TiAl components. The FGM method could meet the expected requirements by eliminating the obvious interface between composite materials in different layers and accommodate materials for specific applications. Meanwhile, the application of powder mixture and LMD technique could reduce cost and lead time of production. This method gives a possibility to effectively manufacture special metallic components that are difficult to fabricate using conventional processing methods. Further, it is important for improving the properties of metallic components and researching new advanced materials by taking use of elemental powder mixture.

The outcomes of the above research topics are expected to advance the knowledge of using elemental powder mixture in LMD process for advanced metallic components fabrication. The technical developments may benefit not only the area of component fabrication, but also other areas such as part repair engineering, aerospace and automation engineering, and additive manufacturing.

1.3. ORGANIZATION OF DISSERTATION

In this dissertation, four major developments are presented and organized as shown in Figure 1.1. These four papers research the same core topic of LMD manufacturing from elemental powder mixture, while each of them has a different focus. Paper I and II focus on the strategy for fabrication of metallic components using elemental power mixture via LMD technique. These two papers present the theories, methodologies, and implementation of the deposition process. This method is helpful for making qualified

target metallic components with economical elemental powder mixture efficiently. Paper III emphasized the application improvement of elemental powder mixture to fabricate novel materials by LMD method. In order to develop innovative metallic alloys with superior metallic properties, the elemental powder mixture is used for laser metal deposition to improve the properties of metallic components and reduce cost. Paper IV developed an FGM path for metal deposition effectively. The FGM method, powder mixture, and LMD technique are used to fabricate metallic components in the process. The focus of this topic is to broad the impact of powder mixture and realize the fabrication of advanced metallic components during the deposition process.

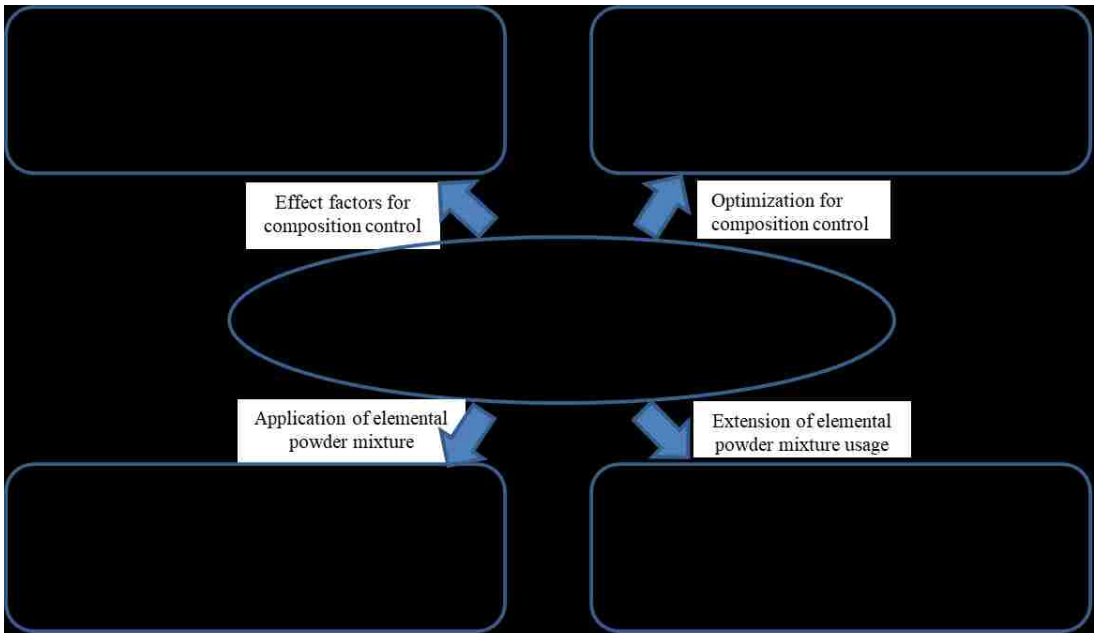

Figure 1.1. Framework of this dissertation

PAPER

I. EFFECT OF POWDER PARTICLE SIZE ON THE FABRICATION OF TI-6AL-4V USING DIRECT LASER METAL DEPOSITION FROM ELEMENTAL POWDER MIXTURE

Xueyang Chen[1], Lei Yan[1], Wei Li[1], Frank Liou[1], and Joe Newkirk[2]

[1]Department of Mechanical and Aerospace Engineering,
Missouri University of Science and Technology, Rolla, MO 65409
[2]Department of Materials Science and Engineering,
Missouri University of Science and Technology, Rolla, MO 65409

ABSTRACT

Direct Laser Metal Deposition (LMD) was used to fabricate thin-wall Ti-6Al-4V using the powder mixture of Ti-6 wt.%Al-4 wt.%V. Scanning electron microscopy (SEM), optical microscopy (OM) and energy dispersive spectroscopy (EDS) were employed to examine the chemical composition and microstructure of the as-deposited sections. Vickers hardness tests were then applied to characterize the mechanical properties of the deposit samples which were fabricated using pre-mixed elemental powders. The EDS line scans indicated that the chemical composition of the samples was homogenous across the deposit. After significant analysis, some differences were observed among two sets of deposit samples which varied in the particle size of the mixing Ti-6wt.%Al-4wt.%V powder. It could be found that the set with similar particle number for Ti, Al and V powder made composition much more stable and could easily get industry qualified Ti-6Al-4V components.

Keywords: Laser metal deposition; Ti-6Al-4V; Elemental powder mixture

1. INTRODUCTION

Laser Metal deposition is an additive manufacturing technique. The applications of this technique include coatings, rapid prototyping, tooling, and refurbishment. As shown in Figure 1.1., laser deposition uses a focused laser beam as a heat source to create a melt pool on an underlying substrate. Powder material is then injected into the melt pool through nozzles. The incoming powder is metallurgically bonded to the substrate upon solidification [1-7]. Conventionally, Direct Laser Deposition (DLD) manufactured parts by adding materials layer by layer using pre-alloyed powder. In the pre-alloyed powder, each individual powder particle has the composition of the desired alloy composition in the final part [8]. But sometimes, it is more flexible to use the mixed elemental powder to develop products. In the elemental powder mixture, each individual powder particle only has the composition of a single element present in the desired final alloy composition, but the blend of the total elemental powder forms the desired final alloy composition [8]. In this study, the material of both powder and substrates is Ti-6Al-4V alloy, which is widely used in the aerospace industry and especially suitable for laser processing. Owing to high cost, this titanium alloy is usually developed by near-net-shape Powder Metallurgy (PM) methods such as laser deposition. Ti-6Al-4V is still classified as one of the extremely difficult-to-machine materials using conventional machining which makes DLD an ideal manufacturing process for the same [9].

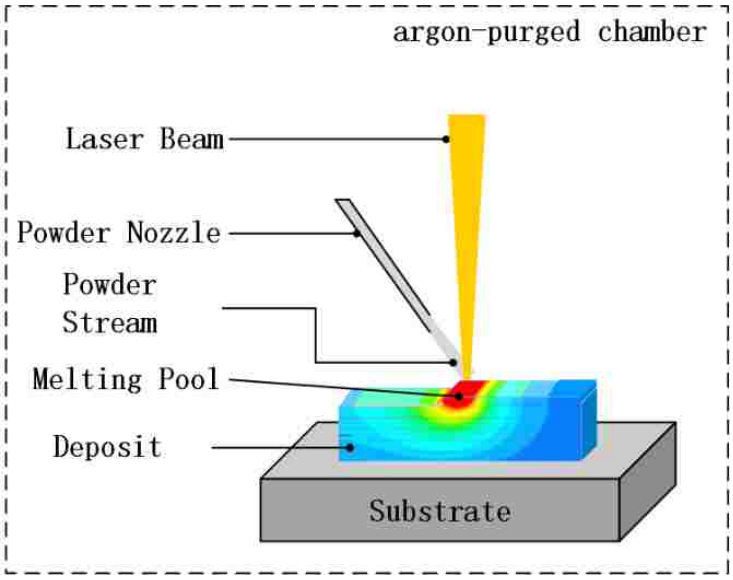

Figure 1. 1. Schematic of the MST-LAMP DLD system [10]

2. EXPERIMENTAL PROCEDURES

Elemental powders used in this study were titanium, aluminum, and vanadium. The elemental powders were characterized to confirm information provided by suppliers and also to determine particle shape and size. By understanding the size distribution and shape of particles, observations and any findings in deposits could potentially be correlated with particle shape or size. Images were taken using a Hitachi S4700 SEM and image analysis was performed using the ImageJ software.

Figure 2.1. shows the SEM images and size distribution of Titanium, Aluminum and Vanadium powder. Titanium powder, grade Ti-109, was purchased from Atlantic Equipment Engineers for use in deposition of Ti-6Al-4V alloys. This powder, grade Ti-109, was listed as being 99.7% and of -100 mesh (<149 μm) size. A SEM micrograph of

the titanium powder can be seen in Figure 2.1. (a) and indicates significant complexity in particle shape. This makes it difficult for the automatic particle analysis software in ImageJ to accurately outline individual particles and calculate their surface area. While this analysis may not give precise measurements, trends in particle size and distribution can be observed. From the resulting software analysis, an average particle size of 106 μm was determined. The elemental aluminum powder, grade Al-103, was produced by Atlantic Equipment Engineers. The purity of the powder was listed as 99.8%. Using similar software analysis gave the Al-103 an average particle size of 165 μm. The elemental vanadium powder, grade VA-103, was purchased from the Atlantic Equipment Engineers with a powder purity of 99.8%. A SEM micrograph of the vanadium powder can be seen in Figure 2.1. (c) and the average size of this powder was 175 μm.

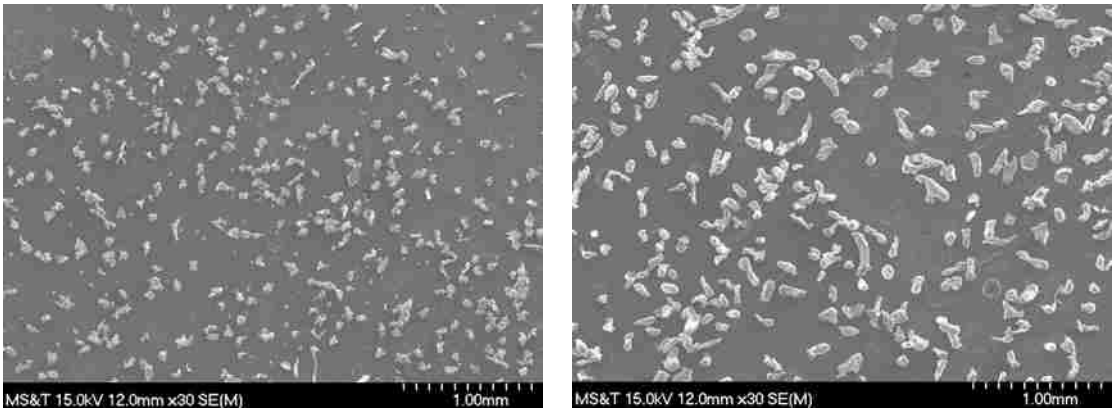

a) Titanium powder SEM image b) Aluminum powder SEM image

Figure 2.1. The SEM images and size distribution of Titanium, Aluminum and Vanadium powder [10]

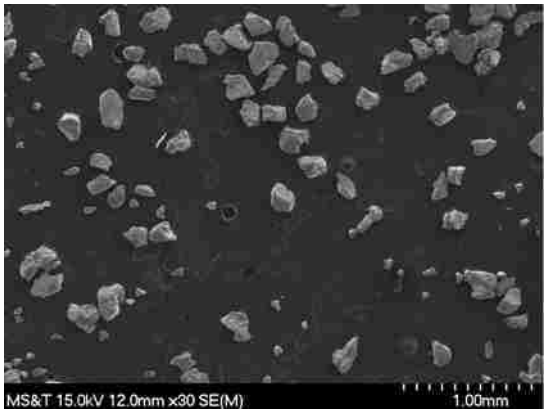

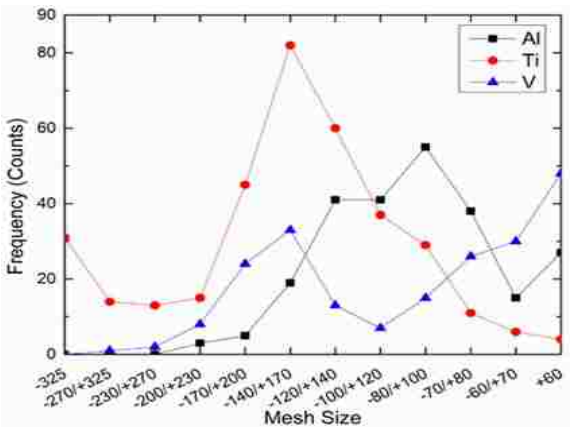

c) Vanadium powder SEM image

d) Particle size distribution

Figure 2.1. The SEM images and size distribution of Titanium, Aluminum and Vanadium powder [10] (cont.)

Before the deposition process began, the elemental powder mixes were prepared. Powders were weighed out according to desired alloy composition in a glove box under an argon atmosphere and placed in a sealed bottle. The powder mixture was a representative of the Ti-6Al-4V alloy. After the desired composition was obtained, the bottle was placed in a Turbula® mixer for 20 minutes. A 1KW Nd: Yag laser was used in this study to deposit these elemental alloy powders. The laser has a wavelength of 1024 nm and approximate 1mm spot size at a 750 mm focal length. To ensure uniformity, thin wall samples with 30 mm track length were deposited on Ti-6Al-4V substrates during the study. Also, all the substrates were 2 inches long, 0.5 inch wide, and 0.25 inch thick. Before deposition, a preheating process was performed by using the laser across the surface of the substrate with 1kW power and without powder. The preheating process was used to form a melt pool on the substrate and clean the surface of the substrate off of scale buildup and other

impurities and surface imperfections. This research theorizes that this pre-heat and clean-up will enable conductive metallurgical bonding of the powders with the substrates.

The commercially irregular pure Ti, Al, and V powders were weighed out and two sets of powder blends were prepared to facilitate similar particle acceleration and similar particle number. It is believed that this will enable a relatively uniform shape of the deposit from top to bottom using the laser deposition system. Ti, Al, and V powders were mixed with the designated weight percentage ratio of 90:6:4 to get target material Ti-6Al-4V. Laser transverse speed was set at 1000 mm/min for all the paths. For laser power, the high normal value of 1 kW was first selected to generate melt pool and then laser power was dropped to and kept stable at 450 W (after 10 layers) to maintain a stable melt pool. While depositing the material, uniformity was ensured in the deposition parameters of travel speed, powder feed rate, and layer thickness constant from test to test. This would lead to an unbiased comparison between different depositions by using similar powder particle and similar powder particle number. Using the analysis, the research theorizes that optimized parameters can be determined in the results for different deposits.

During the laser deposition process, powder blends with the designated weight percentage ratio were injected into the melt pool through the nozzle. To confirm to get target material with the original weight percentage ratio, each element in the blend with the desired composition needs to be melted at the same time. The powder particles had the same initial speed when they went into the nozzle. So particle acceleration is a key factor for composition control. According to the fluid mechanics [11], the particle acceleration is inversely proportional to the particle density and the square of powder diameter, which could be expressed as $a \propto 1/(\rho * D^2)$. Also, particle size for each element in powder blend

has a relationship with the particle number. So particle size of each element could be changed to control the composition in the final part. Then the hypothesis proposed in this research is proved using experiments design around two sets of data namely

Set 1: A comparative study of the acceleration of the elemental powder particles (Table 2.1.).

Set 2: A comparative study of the number of particles in each elemental powder (Table 2.2.).

Among the two sets of experiments conducted, the appropriate particle size of Ti, Al and V powder has been selected according to the particle diameter listed in Table 2.1., it shows the particle size and calculated acceleration ratio of Ti, Al and V powder. In this experiment, Ti, Al, V elemental powder has the similar particle acceleration during the process. Similarly, after choosing suitable particle size for set 2, corresponding particle number ratio of Ti, Al, V powder could be calculated in Table 2.2. In this set, Ti, Al, V elemental powder has the similar particle number during the process. These two sets of experiments were chosen to study which factor, among particle acceleration and particle number, would affect an as-built part's final chemistry composition.

Table 2.1. Particle Size and Acceleration Ratio in Set 1

Irregular powder	**Density (kg/m^3)**	**Diameter (μm)**	**Acceleration ratio**	**Number ratio**
Ti	4507	112	1	19.2
Al	2700	133	1.18	1.3
V	6110	96	1.06	1

Table 2.2. Particle Size and Number Ratio in Set 2.

Irregular powder	**Density (kg/m^3)**	**Diameter (μm)**	**Acceleration ratio**	**Number ratio**
Ti	4507	147	1	2.4
Al	2700	94	0.25	1
V	6110	63	0.25	1

After deposition, longitudinal samples were cut off using the EDM machine and mounted for grinding and polishing. Kroll's Reagent consisting of 92 ml distilled H2O, 6 ml HNO3, and 2 ml HF was used for etching. To research the microstructure characteristic and composition in the elemental powder deposits, energy dispersive spectroscopy (EDS) line scans were performed using Hitachi S4700 and FEI Helio 600 scanning electron microscope (SEM). Also, optical microscopy was used to assess the microstructure in the samples. Comparison of the mechanical properties between the two sets of different samples was also conducted. The Vickers hardness measurements were taken with a Struers Duramin micro-hardness tester. 9.8kg load with a dwell time of 10 seconds was applied during the test hardness procedures.

3. RESULTS AND DISCUSSION

3.1. VICKERS HARDNESS & EDS TEST

Figure 3.1. shows the composition distribution and Vickers hardness of the deposited sample from elemental powders of Set 1 whose three elements of Ti, Al, and V have the similar particle acceleration. Ti-6Al-4V substrate Vickers hardness was first taken

near the bottom edge that is away from heat affected zone (HAZ) and found to be 352.44±15.41 HV. It was observed that the Vickers hardness values increased as it progressed into the HAZ from the substrate. In the deposit zone, there was a temporary increase for the first several layers, then a decrease and stabilization from the middle to the top of the deposit.

For the deposited samples using mixed powder of Set 1, area scan and line scan were employed to investigate the composition distribution along the build height direction. Figure 3.1. shows the EDS result of the deposit. The weight percentage of Ti, Al and V could be found in the image in the left figure of Figure 3.1. Al and V curves were focused on and showed their weight percentage variation against the position in the image on the right. Two marked zones in this figure mean industry qualified Al and V weight percentage for Ti-6Al-4V, which is Al ranges from 5.5-6.75% and V ranges from 3.5-4.5%. At deposit height, Al and V weight percentage showed that the values varied outside the qualified range, which means the as-deposit alloy was not the targeted material Ti-6Al-4V. There was some powder loss when the powder mixture went through the nozzle, so it was supposed that less powder in the blend especially for Al and V powder because of the low volume of them. This would lead to the result that the weight percentage of Al and V along build height direction vary a lot.

Figure 3.2. shows the composition distribution and Vickers hardness of the deposited sample from elemental powders of Set 2 whose three elements of Ti, Al, and V have similar particle number. Also, Ti-6Al-4V substrate Vickers hardness was first taken near the bottom edge that is away from heat affected zone (HAZ) and found to be 359.11±13.78 HV. In this case, it was observed that the Vickers hardness values decreased

with progress into the HAZ from the substrate side. In the deposit zone, there was an increase for the first several layers and stabilization beyond that.

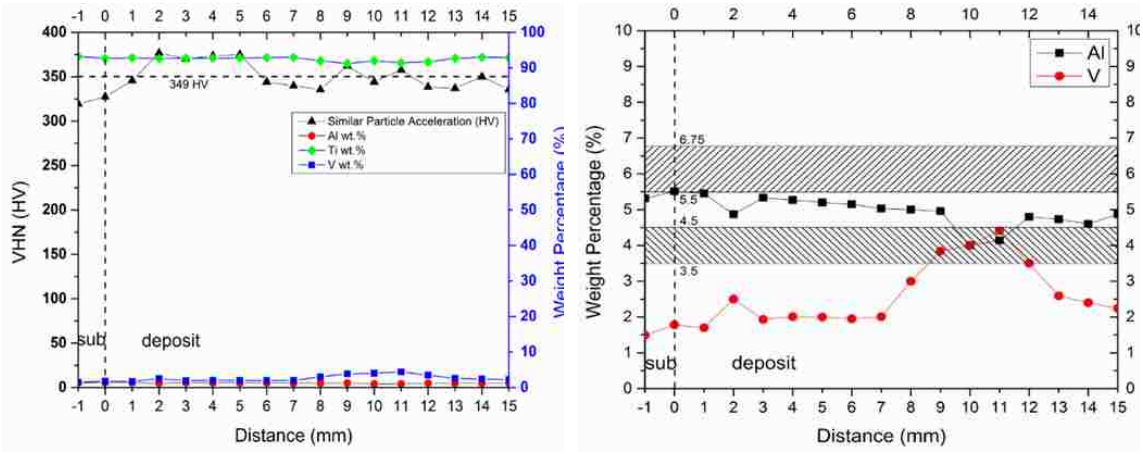

Figure 3.1. Composition distribution & Vickers Hardness along build height direction of Set 1

For the newly deposited samples using mixed powder (Set 2), area scans and line scans were also employed to check the composition distribution along the build height direction. Figure 3.2. shows the EDS results of the deposits. The weight percentage of Ti, Al and V could be found in the image on the left of Figure 3.2. Al and V curves were focused on and showed their weight percentage variation in the image on the right of Figure 3.2. Two marked zones in the right figure mean industry qualified Al and V weight percentage for Ti-6Al-4V. It can be seen that the deposit had qualified Al and V weight percentage and get close to the maximum limit of industry qualified Ti-6Al-4V, which means industry qualified Ti-6Al-4V has been made. From this, it can be concluded that powder number for each of the elements in the blends is a key factor towards the

composition acquired in the final part. It could be found that similar particle number made composition much more stable and close to industry qualified Ti64. The research theorizes that the increase in the volume of Al and V in the set 2's powder blends increases the probability of those two elements particles falling into melt pool.

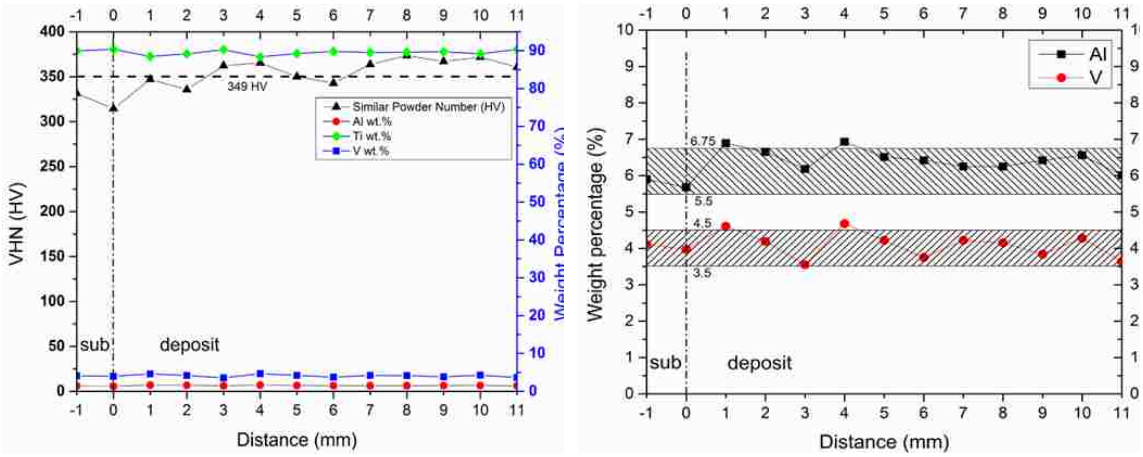

Figure 3.2. Composition distribution & Vickers Hardness along build height direction of Set 2

Figure 3.3.(a) showed the line scan of the deposited sample from elemental powders of Set 1 whose three elements of Ti, Al, and V have similar particle acceleration. Figure 3.3.(b) showed the line scan of the deposited sample from elemental powders of Set 2 whose three elements of Ti, Al and V have similar particle number. Line scan was shown in Figure 3.3.(a) to define composition homogeneity along the build height direction. Thus, it can be known that similar particle acceleration could not guarantee a homogeneous chemistry distribution throughout the deposit from Figure 3.3.(a). Also, Line scan was

shown in Figure 3.3.(b) to define composition homogeneity along the build height direction which shows that the distribution is homogenous for the deposit.

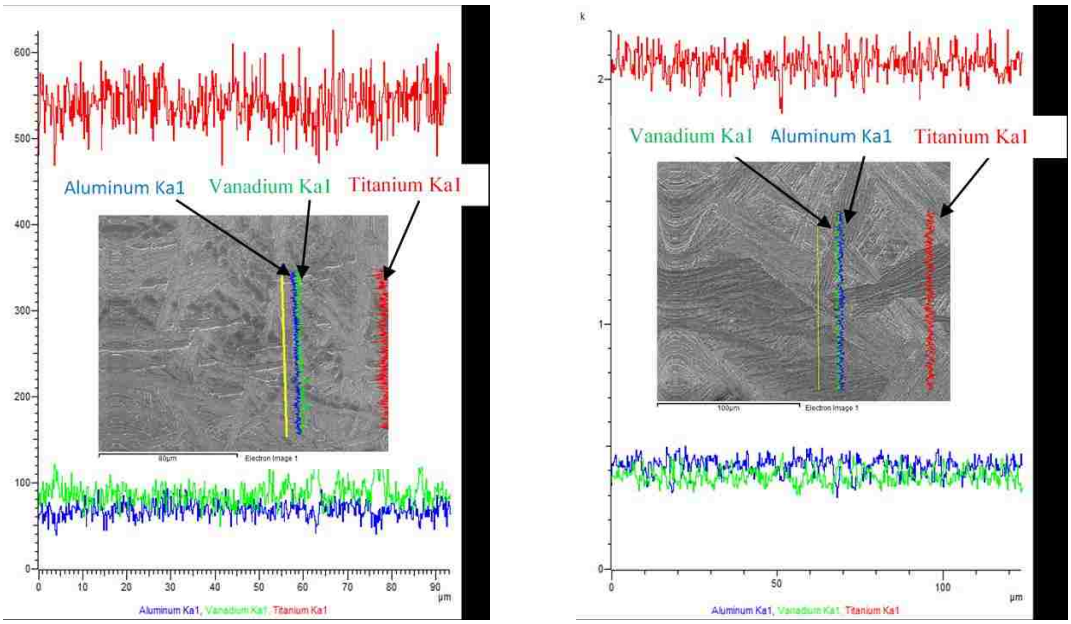

a) Similar particle acceleration b) Similar particle number

Figure 3.3. Line scan of the deposited samples

3.2. MICROSTRUCTURE

Figure 3.4. shows the microstructure of deposited Ti-6Al-4V from elemental powder mixture with the similar particle acceleration at the same laser power and laser transverse speed. The optical microscope images captured from the bottom part, middle part and top part of the melt pool (Figure 3.4. (a) to (c)) in the deposit contained basketwave, colony, and martensite microstructure respectively. Figure 3.4. (a) showed the finer

microstructure could be observed in the bottom part compared with the middle and top part of the deposit. Also, a steady state could be observed from middle part to top part and there were limited differences in the microstructure between them. In these two zones, the Widmanstätten Basketwave is the main type of microstructure that could be found. It tends to form with an increasing cooling rate from the β-phase field [12-13].

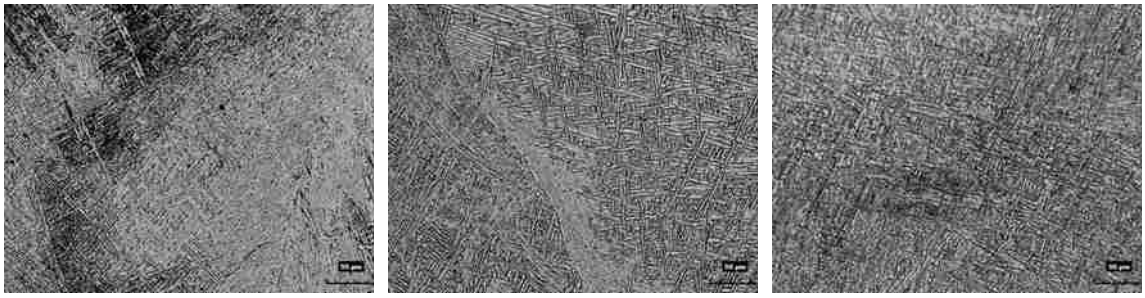

a) Bottom of the deposit b) Middle of the deposit c) Top of the deposit

Figure 3.4. Microstructure of the deposits using elemental powders of Set 1

Analyses of these microstructures revealed that the smaller grain sizes were achieved closer to the substrate in the deposit. The reason was the proximity to the substrate, increased the cooling rate, which would lead to a finer microstructure [14]. The same phenomenon was observed in the microstructure of the deposited samples from the elemental powder mixture with the similar particle number of Set 2. Therefore, it was concluded that the steady state section tends to have the lower cooling rate, which would lead to the formation of coarser microstructure [15]. Figure 3.5. shows the microstructure of deposited Ti-6Al-4V from elemental powder mixture with the similar particle number

using the same laser power and laser transverse speed. Also, a steady state could be observed from middle part to top part and Widmanstätten Basketwave is the main type of microstructure that could be found.

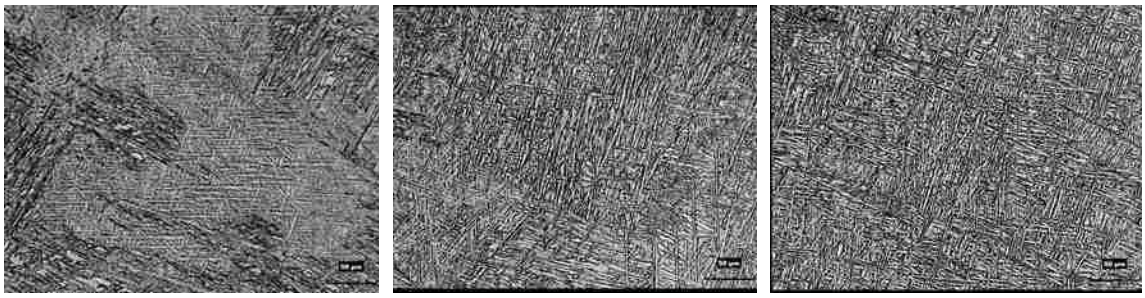

a) Bottom of the deposit b) Middle of the deposit c) Top of the deposit

Figure 3.5. Microstructure of the deposits using elemental powders of Set 2

4. CONCLUSIONS

The blended elemental powder can be used in the direct laser deposition process to offer a variety of cost-effective possibilities for near-net-shape manufacture and functionally graded materials. The finer microstructure could be observed in the bottom part of the deposit compared with the steady state in the middle and top part of the deposit. The Vickers hardness could fluctuate at the first several layers of the deposit and then stayed stable at the top layers of the deposit. Particle number for each element in powder blends is a key factor for composition control in the final part. Similar particle number for Ti, Al and V powder could easily get industry qualified Ti-6Al-4V components.

REFERENCES

[1] Chua, C.K., Leong, K.F., Lim, C.S., Rapid Prototyping: Principles and Applications, 3rd Edition, 2010.

[2] Unocic, R.R. & DuPont, J.N., Composition control in the direct laser deposition process, Metall. Mater. Trans., 34B, pp.439-445, 2003.

[3] Gedda, H., Kaplan, A. & Powell, J., Melt-solid interactions in laser cladding and laser casting, Metall. Mater. Trans., 36B, pp. 683-689, 2005.

[4] Lei, T. C., Ouyang, J. H., Pei, Y. T. & Zhou, Y., Microstructure and sliding wear properties of laser clad TiN reinforced composite coating, Surface Engineering, 12, pp.55-60, 1996.

[5] Kaplan, A. F. H. & Groboth, G., Process analysis of laser beam cladding, Trans. ASME J. Manuf. Sci. Eng., 123, pp. 609-614, 2001.

[6] Watkins, K. G., Achieving the potential of direct fabrication with lasers, Proc. of 3rd Int. Conf. on Laser Assisted Net Shaping, Erlangen, Germany, pp. 25-38, 2001.

[7] Griffith, M. L. et al., Understanding thermal behaviour in the LENS process, Materials and Design, 20, pp.107-113, 1999.

[8] Clayton, Rodney Michael, The use of elemental powder mixes in laser-based additive manufacturing, 2013.

[9] O.M. Ivasishin, V.M. Anokhin, A.N. Demidik, D.G. Savvakin, Cost-Effective Blended Elemental Powder Metallurgy of Titanium Alloys for Transportation Application, 2000.

[10] Lei Yan, Xueyang Chen, Wei Li, Frank Liou, and Joe Newkirk, Direct Laser Deposition of Ti-6Al-4V from Elemental Powder Blends, Proceedings of the Solid Freeform Fabrication, University of Texas, Austin, 2015.

[11] P.M. Whelan, M.J. Hodgeson (1978). Essential Principles of Physics (2nd ed.).

[12] R. Boyer: Metals Handbook: Metallography and Microstructures, ASM, Materials Park, OH, 1985, vol. 9, pp. 458–75.

[13] Bernd Baufeld., Omer Van der Biest., Rosemary Gault, Additive manufacturing of Ti–6Al–4V components by shaped metal deposition: Microstructure and mechanical properties, Materials & Design, Volume 31, Pages S106-S111 , 2010.

[14] Simonelli, M., Y. Y. Tse, and C. Tuck., Microstructure of Ti-6Al-4V produced by selective laser melting, Journal of Physics: Conference Series. Vol. 371. No. 1. IOP Publishing, 2012.

[15] Nassar, Abdalla R., and Edward W. Reutzel., Additive Manufacturing of Ti-6Al-4V Using a Pulsed Laser Beam, Metallurgical and Materials Transactions A46.6 (2015): 2781-2789.

II. COMPOSITION CONTROL ON TI-6AL-4V FABRICATION BY LASER METAL DEPOSITION FROM ELEMENTAL POWDER MIXTURE

Xueyang Chen[1], Sreekar Karnati[1], Yunlu Zhang[1], Lei Yan[1], and Frank Liou[1]

[1]Department of Mechanical and Aerospace Engineering,
Missouri University of Science and Technology, Rolla, MO 65409

ABSTRACT

Laser metal deposition (LMD) technique has been identified as an effective means for economically fabricating custom alloys using blended elemental powder mixtures. However, there are issues that need to be addressed in order to realize the full potential of this approach. The primary issue is the lack of composition control resulting from blend separation and dissimilar flow characteristics of constituent powders. In the current study, the spatial distribution of elemental titanium, aluminum and vanadium powder particles were stochastically modelled. These models indicated the capture efficiency of the melt pool varied with the type and size of the powder. By selecting appropriate powder sizes and compensating for differences in capture efficiencies, a powder blend was designed to successfully achieve the target Ti-6Al-4V (Ti64) composition. The homogeneity of the fabricated material was validated by assessing the weight percentages of the constituent elements using quantitative X-ray Energy Dispersive Spectroscopy (EDS). The assessment involves in-part and part to part comparison of chemistries. Both martensitic and basket weave microstructures were observed in the deposits. The fabricated Ti64 alloy was found to possess a higher hardness in comparison to the commercially procured Ti64 substrate.

Keywords: Ti-6Al-4V; elemental powder mixture; laser metal deposition, stochastic modelling, composition control, modular feedstocks..

1. INTRODUCTION

Ti-6Al-4V (Ti64) alloy is an alpha-beta structure alloy, it is known to exhibit high strength-to-weight ratio in comparison to most of the steel and aluminum based alloys. It is used in more than 50% of the applications requiring titanium, this makes it one of the most popular titanium alloy [1]. It has been widely used in areas such as aerospace engineering, marine equipment, auto industry, and biomaterials [2]. This alloy is an excellent combination of low density, remarkable mechanical strength, excellent corrosion resistance and ductility. These properties also makes it extremely difficult to fabricate Ti64 components using conventional machining methods. Additive manufacturing has been identified as an extremely effective method to fabricate Ti64 component in near net shape geometries. Much of the existing additive manufacturing based research has been done on the fabrication of Ti64 components by using pre-alloyed Ti64 powder. Qiu et al. [3] prepared Ti64 samples by direct laser deposition (DLD) using gas atomized Ti64 powder under various processing conditions. They successfully fabricated large Ti64 structures by optimizing various process parameters. Baufeld et al. used Shaped Metal Deposition (SMD) technology to produce large and dense Ti64 components with different shapes using pre-alloyed powders [7]. Electron Beam Melting (EBM) process was also found to be widely used to fabricate Ti64 alloy components with complex geometries for orthopedic and

dental implants applications [4]–[6]. The laser metal deposition (LMD) technique is an advanced additive manufacturing technology which is capable of fabricating near net shape metallic components in a layer by layer fashion from computer-aided design (CAD) models. This technique is capable of reducing cost by significantly reducing the buy-to-fly ratios and lead times of production. It is therefore particularly beneficial to fabricate Ti64 components using LMD

Conventionally, pre-alloyed powders were used as the feedstock in the LMD manufacturing process. While the possibilities and advantages of using pre-alloyed Ti64 powders are evident, there is a high cost associated with procuring pre-alloyed Ti64. Most of the additive manufacturing technologies involve the use of a high power source such as, laser, electron beam, and welding gun. Owing to the high temperatures associated with the process, vaporization of aluminum is highly probable. Compensating for the loss of aluminum is not feasible while using pre-alloyed Ti64. Fabricating custom compositions of pre-alloyed powder can be significantly expensive. Using elemental powders as modular feedstocks could be the solution for addressing the issues of Ti64 fabrication. By using elemental powder mixtures the procurement cost can be significantly reduced. Also, it is possible to fabricate a multitude of compositions using elemental powder mixtures. This could potentially lead way to the development of innovative alloys through investigation of variety of alloy systems. Additionally, elemental powder mixtures provide the flexibility to fabricate compositionally graded materials by varying the blend ratios of the powder mixture. Some studies have been conducted on the fabrication of advanced materials by using blended powder mixtures. For example, Ye et al. demonstrated a route for low-cost, single-step densification of Ti-6Al-4V by hot pressing of blended powders, commercially

purified Ti (CP-Ti) and Al-40V, allowing the use of low-cost CP-Ti powders and avoiding costly HIP densification [8]. While there are significant advantages to using blended powder mixtures, metal components fabricated from elemental powder mixtures have been identified to have issues of instability and non-repeatability with regards to composition. Collins's [9] research on fabrication of Ti-Al and Ti-Al-Mo indicated that powder size and material density could influence the actual composition of the deposit.

Though the powder characteristics have been found to influence the final composition, currently limited literature exists on means to compensate for this variation. The work previously done by the authors, showed that the number density (number of particles per unit volume) of each element in the powder mixture affects the variation in composition of deposited part. Maximizing the number density of elements by varying the powder size was found to reduce the compositional variation in the deposited material. The authors theorize, by modelling the spatial distribution of the powder particles just above the melt pool, the capture efficiency of melt pool for each constituent elemental powder can be realized. If the post-capture weight percentages of the powders match the intended composition, the deposited material is expected to meet the specification requirements. In this paper, a series of experiments have been performed to estimate the spatial distribution of each type of powder during the deposition process. Based on these distributions, the compensation factors were accordingly calculated to design a feedstock that could attain calculated post-capture weight percentages which would meet specification requirements. The fabricated material was then analyzed for compositional variation to ascertain the validity of the proposition.

2. MATERIALS AND METHODS

2.1. MATERIAL PREPARATION

Under the current study, elemental powders of titanium, aluminum, and vanadium were used as feedstocks. Blends of these powders were made by mixing these elements to achieve different compositions of Ti-Al-V alloys. Titanium was purchased from Advanced Powders & Coatings (AP&C). The elemental aluminum powder was produced by Atlantic Equipment Engineers, and vanadium powder was from CNPC Company. Figure 2.1. shows the powder morphology of titanium, aluminum, and vanadium powder using Helios Nanolab 600 SEM (FEI Company, Hillsboro, OR, United States). The particle size definitions of Ti, Al, and V powders are listed in Table 2.1. The Ti-6Al-4V plate was used as the substrate material for these depositions, and substrates were prepared to the dimensions of 2× 0.5 × 0.25 in. A stainless steel sieve set including five sieve sizes (45 microns, 75 microns, 105 microns, 125 microns, and 150 microns) was used to separate the three kinds of powder particles into different groups based on the sizes of the particles for further study.

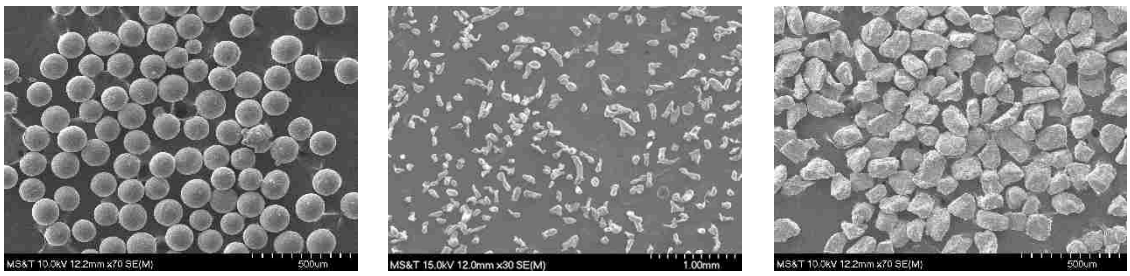

a) Titanium powder image b) Aluminum powder image a) Vanadium powder image

Figure 2.1. The morphology images of Titanium, Aluminum and Vanadium powder

Table 2.1. Particle size of the original materials

Materials	US Standard Mesh
Ti	−100/+325
Al	−100
V	−100

2.2. DEPOSITION SYSTEM

In this study, a 1 kW continuous wave fiber laser with a wavelength of 1064 nm was used to deposit the elemental powder mixture. A melt pool spot size of approximately 2 mm was obtained through a lens of 750 mm focal length. A commercial powder feeder was used to supply powder particles. A ceramic tube nozzle was used in conjuncture with a CNC (Computer Numerical Control) table to facilitate movement and perform deposition. Argon gas was used to implement an inert atmosphere and was also used as a carrier gas to deliver the powder mixture to the melt pool.

The schematic layout of the LMD system is shown in Figure 2.2. LMD deposition is an additive manufacturing technique capable of fabricating complicated structures with superior properties. The applications of this technique include coatings, rapid prototyping, tooling, repair, etc. LMD uses a focused laser beam as a heat source to create a melt pool into which powder feedstock is injected. The powder material is metallurgically bonded to the substrate through solidification.

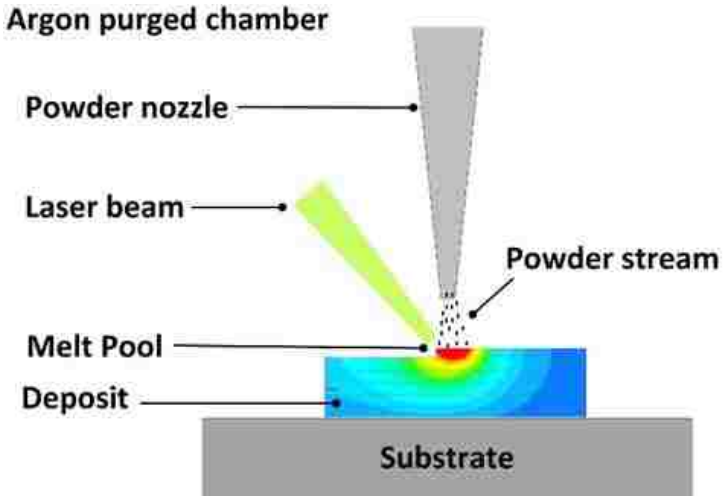

Figure 2.2. Schematic layout of the LMD (Laser Metal Deposition) system

2.3. EXPERIMENTAL PROCEDURE

2.3.1. Powder Distribution Experiment Set-up. In this research, three kinds of powder have been fed into the powder feeder individually in order to get their spatial distribution on the substrate. This powder distribution experiment set-up is shown in Figure 2.3. (a). A transparency film was spread out epoxy resin. One piece of aluminum alloy plate pasted with the transparency film on it was set on the stage of CNC machining system. During the process, the nozzle of the ceramic tube could spray powder on the sticky epoxy resin of the transparency film along a designed path. Figure 2.3. (b) shows the solidified epoxy resin layer with captured powder. The moving path is a zig-zag shape as shown in this figure. After the resin got solidified, the powder distribution pattern on the substrate was shown in this Figure 2.3. (c). Take an image from part of the solidified epoxy resin layer as shown in Figure 2.3. (c). According to the image analyses code of Yunlu Zhang, the powder particle positions in the observed zone could be obtained. The particle

distributions could be displayed by analyzing the capturing powder image. Figure 2.3. (c) shows the un-sieved Ti powder particle distribution, and Table 2.2. shows the portion percentages and standard deviations for its distribution. Because the melt pool is 2mm wide, the probability of powder particles that falling in the melt pool could be calculated according to the distribution. Using the same way, the powder distributions for particles within different size ranges could be obtained.

Take an image from part of the solidified epoxy resin layer as shown in Figure 2.3. (c). According to the image analyses code of Yunlu Zhang, the powder particle positions in the observed zone could be obtained. The particle distributions could be displayed by analyzing the capturing powder image. Figure 2.3. (c) shows the un-sieved Ti powder particle distribution, and Table 2.2. shows the portion percentages and standard deviations for its distribution. Because the melt pool is 2 mm wide, the probability of powder particles that falling in the melt pool could be calculated according to the distribution. Using the same way, the powder distributions for particles within different size ranges could be obtained.

Our previous research revealed that the particle number for each element in powder blends is a key factor for composition control in the final part [10]. It can be deduced that the composition of deposit part can be affected by the spatial distribution of different elemental powders in the mixture. By keeping the same size of the melt pool, the composition of the samples deposited by elemental powder mixture could be controlled by changing the powder volumes. In this way, it is necessary to get the spatial distribution of different powder particles. The powder distribution images were taken to investigate the powder spay locations. After analyzing the positions of individual particles, the powder

flow distributions became visible. By sieving the particles to different size ranges, the capture efficiency for the powders could be improved by optimizing the ratio of different powders. The powder capture rate is the ratio of the powder mass fed into the part to the total powder mass used during the LMD process.

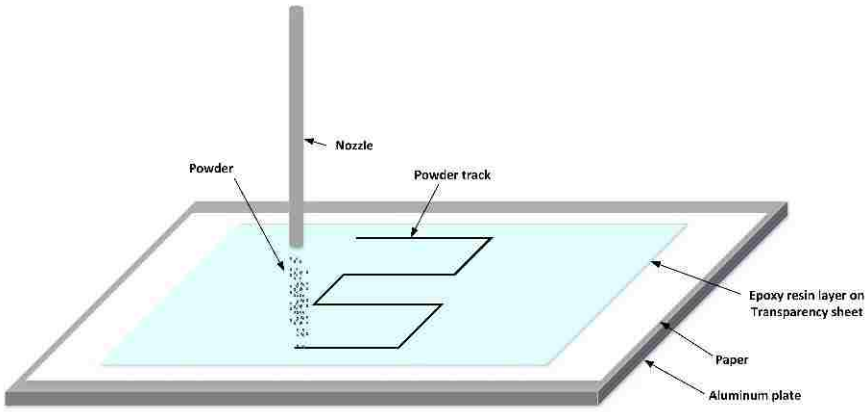

(a)

(b)

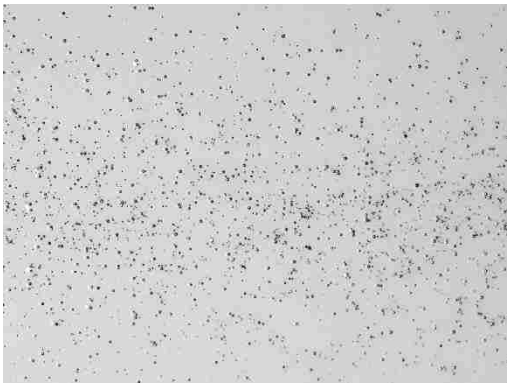

(c)

Figure 2.3. (a) Powder distribution experiment set-up, (b) Solidified epoxy resin layer on the transparency film, and (c) The powder distribution pattern

Table 2.2. Probability distribution data of un-sieved titanium powder.

Powder	Powder Groups	Portion 1	Standard derivation (σ_1) (μm)	Powder probability within 2mm range
Ti	Un-sieved powder	1	4084.782	0.193862

2.3.2. Powder Distribution Experiment Design Theory. Our previous research revealed that the particle number for each element in powder blends is a key factor for composition control in the final part [10]. It can be deduced that the composition of deposit part can be affected by the spatial distribution of different elemental powders in the mixture. By keeping the same size of the melt pool, the composition of the samples deposited by elemental powder mixture could be controlled by changing the powder volumes. In this way, it is necessary to get the spatial distribution of different powder particles. The powder distribution images were taken to investigate the powder spay locations. After analyzing the positions of individual particles, the powder flow distributions became visible. By sieving the particles to different size ranges, the capture efficiency for the powders could be improved by optimizing the ratio of different powders. The powder capture rate is the ratio of the powder mass fed into the part to the total powder mass used during the LMD process.

2.3.3. Deposition and Analyses Process. Powders were weighed for desired alloy compositions in a glove box under an argon atmosphere and sealed in bottles. The as-blended weight percentages of these powder mixtures can be represented by Ti-xAl-yV (x,y could be decided according to powder distribution results). These bottles were then

shaken using a Turbula® mixer (Glen Mills Inc., Maywood, NJ, United States) for 20 min to obtain thorough mixing and homogeneity within the powder blends.

Thin wall claddings were fabricated by performing single melt pool, layer by layer deposition. To ensure perfect bonding, before deposition, a preheat scan was performed by running the laser across the surface of the substrate at 1 kW power. The preheating process was used to heat up the substrate and rid the surface of the substrate from oxide scale buildup, surface impurities, and, surface imperfections. Laser transverse speed was set at 600 mm/min for all the depositions. The initial 10 layers of deposition carried out a power to 1 kW to ensure perfect bonding with the substrate. The rest of the deposition was carried at a power of 400 W. The same deposition scheme and parameters were used for all the depositions.

After deposition, vertical transverse sections were cut using a wire Electro-Discharge Machine (wire-EDM, Hansvedt Industries Inc., Rantoul, IL, United States) and mounted in Bakelite for grinding and polishing. Kroll's Reagent, consisting of 92 mL H_2O, 6 mL HNO_3, and 2 mL HF was used for etching. Hirox optical microscope was used to perform microstructure imaging. Helios Nanolab 600 SEM (FEI Company, Hillsboro, OR, United States) equipped with an Oxford Energy Dispersive Spectrometer and HKL Electron Backscatter Diffraction system was used to get the chemical compositions. The Vickers hardness measurements were performed on the two different compositions using a Struers Duramin micro-hardness tester(Struers Inc., Cleveland, OH, United States). Press load of 9.81 N and load time of 10 s was used during the hardness tests.

3. RESULTS AND DISCUSSION

3.1. POWDER DISTRIBUTION

After exiting the nozzle, the powder particles are drawn downward the plate. Powder distribution images were taken to investigate the probability functions. In detail, the probability plot and density function figures of Ti, Al, and V powder are presented in Figure 3.1., 3.2., and 3.3. respectively. The measurement results are listed in Table 3.1.

In Figure 3.1., Ti powder distributions of different size groups (un-sieved, 0-45 μm, 45-75 μm, 75-105 μm, 105-125 μm, >125 μm) are shown here. It can be seen that each group of powder spreading function indicated one normal distribution. All the powder groups have different standard derivations. Al and V powder distributions are shown in Figure 3.2. and 3.3. For some smaller size group of powder particles, they followed a bi-model normal distribution. Their portion percentages and respective standard derivations are all shown in Table 3.1.

According to this, the probabilities for the powder particles blown into the melt pool (a 2mm spot) of different size groups could be calculated and tabulated in Table 3.1. To further investigate the case, the deposition experiments were carried out using a blend of Ti, Al, and V powders based on the powder particle distributions. It could be known that the powder volume in the melt pool could be expressed as $V_m = M_t/\rho$, M_t is the target mass of powder, ρ is the density of powder. The powder volume is proportional to the powder particle number when each kind of powder particle volume is close. The powder capture rate R is the ratio of the powder mass fed into the part to the total powder mass used during the LMD process. R is the powder probability within 2mm melt pool in this case.

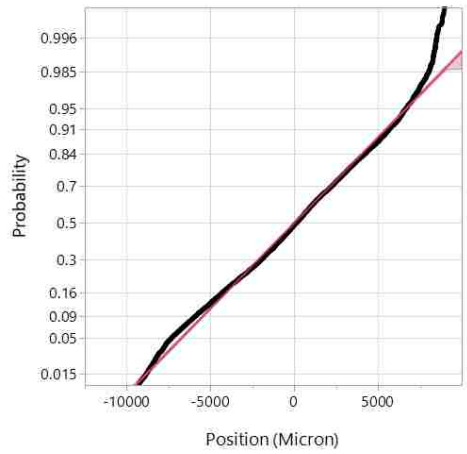

(a) Probability plot of un-sieved Ti powder

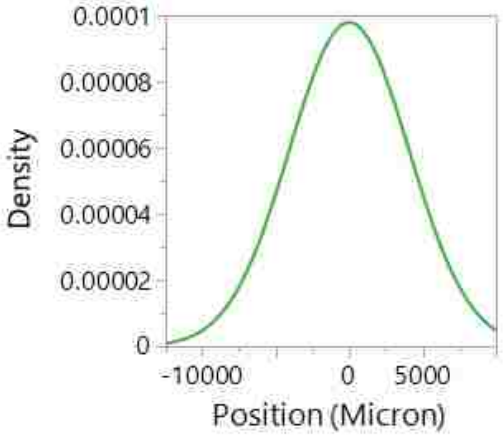

(b) Probability density function for un-sieved Ti powder

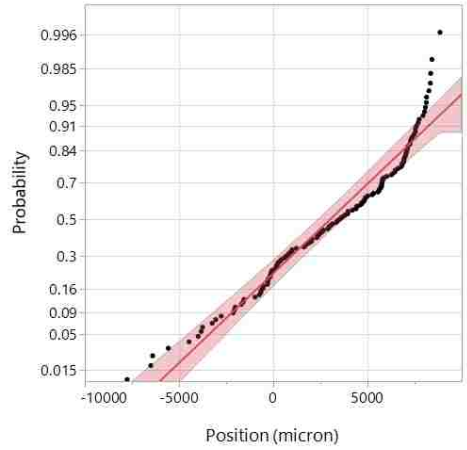

(c) Probability plot of 0-45 µm Ti powder

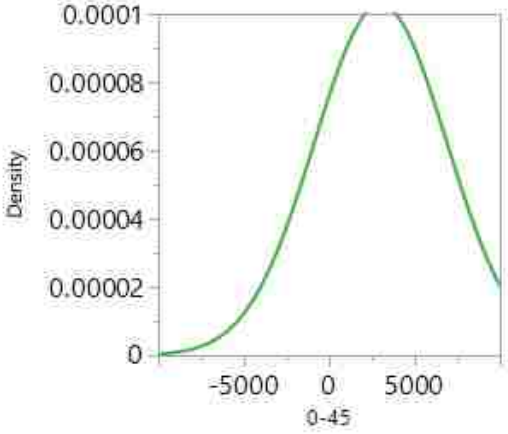

(d) Probability density function for 0-45 µm Ti powder

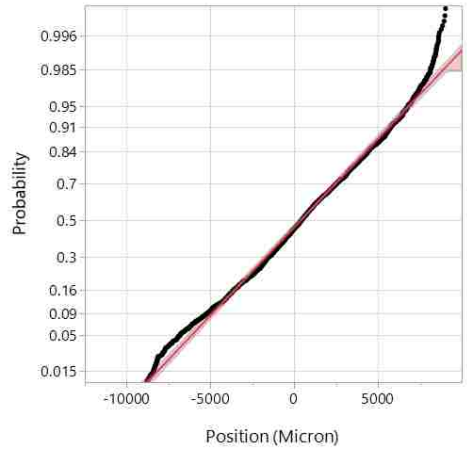

(e) Probability plot of 45-75 µm Ti powder

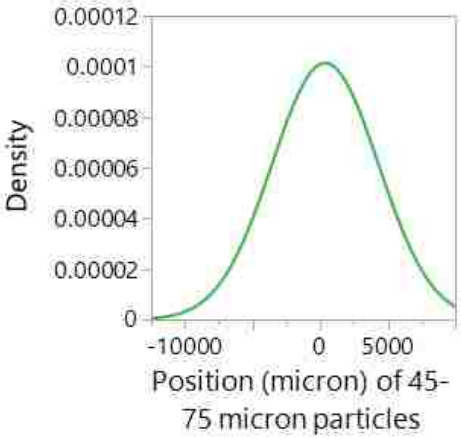

(f) Probability density function for 45-75 µm Ti powder

Figure 3.1. Probability Distribution for Ti powder of all size groups

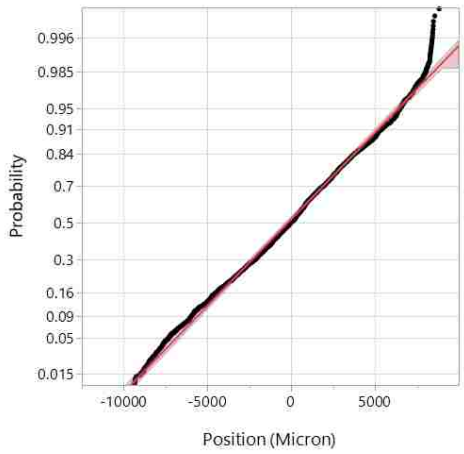

(g) Probability plot of 75-105 µm Ti powder

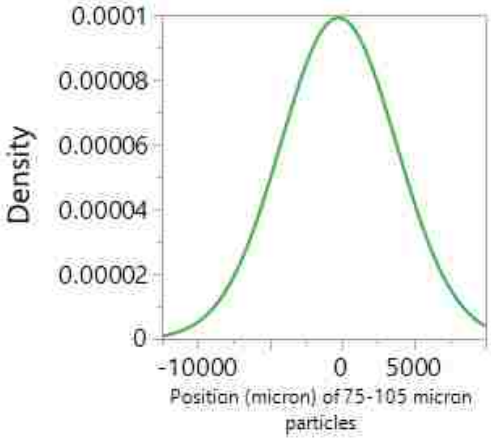

(h) Probability density function for 75-105 µm Ti powder

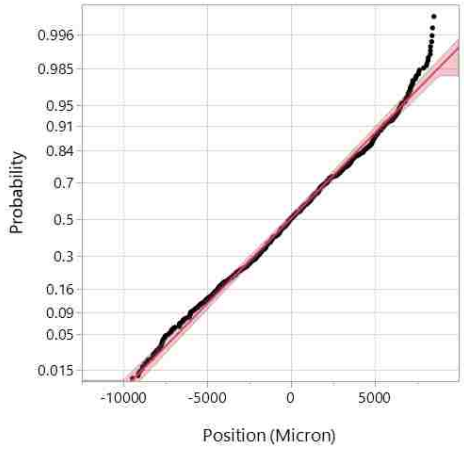

(i) Probability plot of 105-125 µm Ti powder

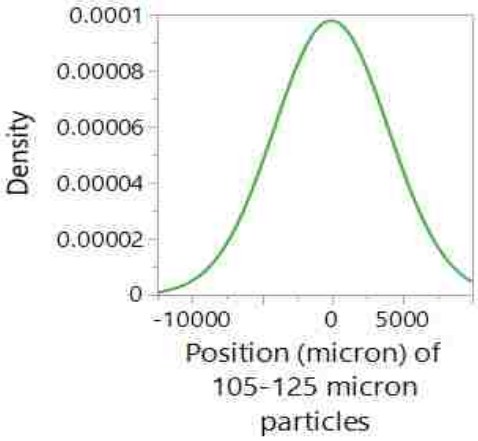

(j) Probability density function for 105-125 µm Ti powder

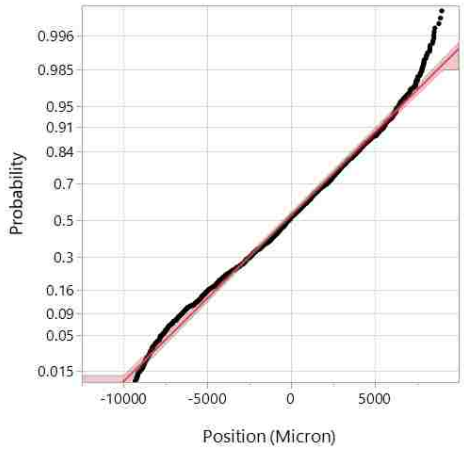

(k) Probability plot of >125 µm Ti powder

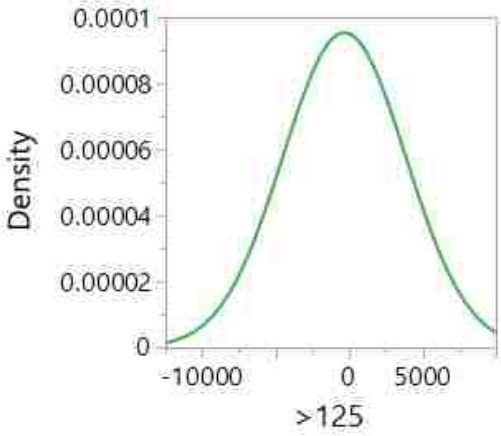

(l) Probability density function for >125 µm Ti powder

Figure 3.1. Probability Distribution for Ti powder of all size groups (cont.)

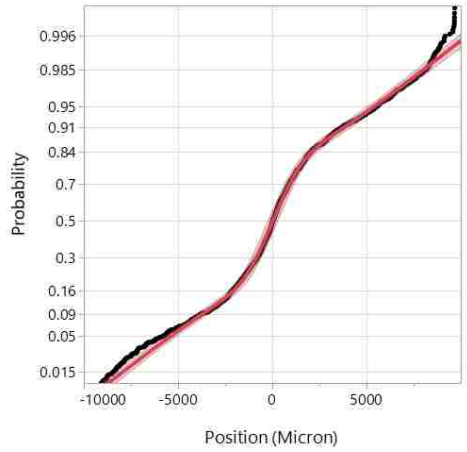

(a) Probability plot of un-sieved Al powder

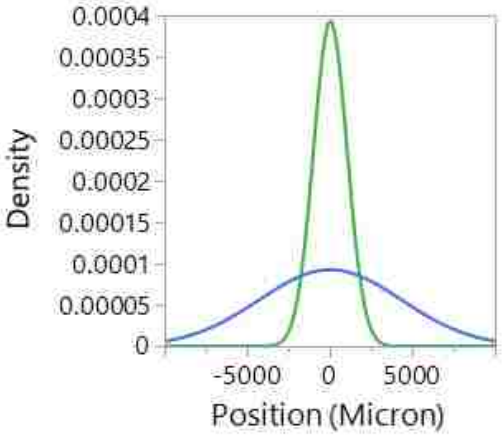

(b) Probability density function for un-sieved Al powder

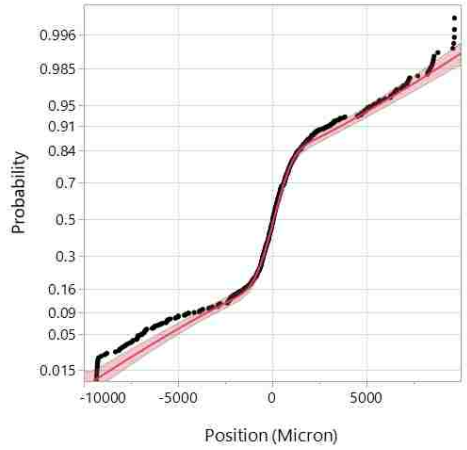

(c) Probability plot of 0-45 µm Al powder

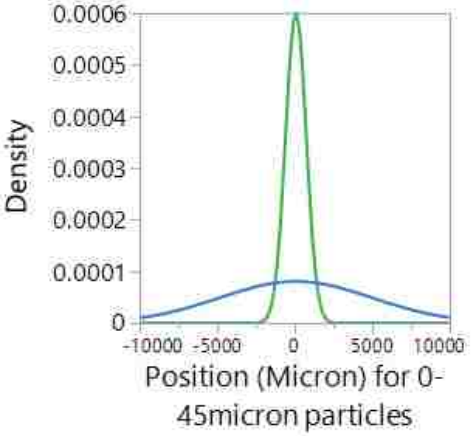

(d) Probability density function for 0-45 µm Al powder

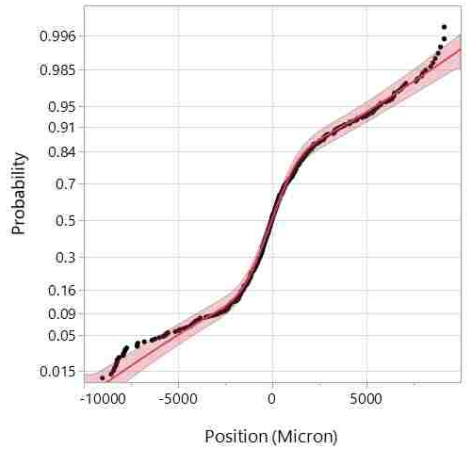

(e) Probability plot of 45-75 µm Al powder

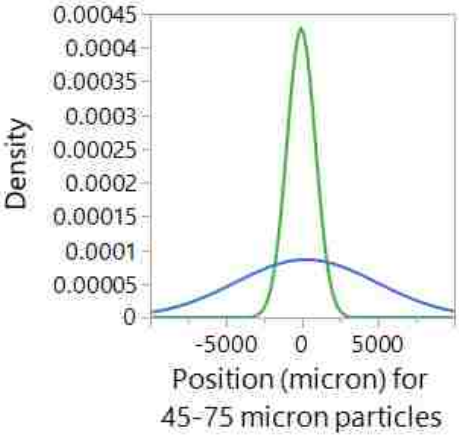

(f) Probability density function for 45-75 µm Al powder

Figure 3.2. Probability Distribution for Al powder of all size groups

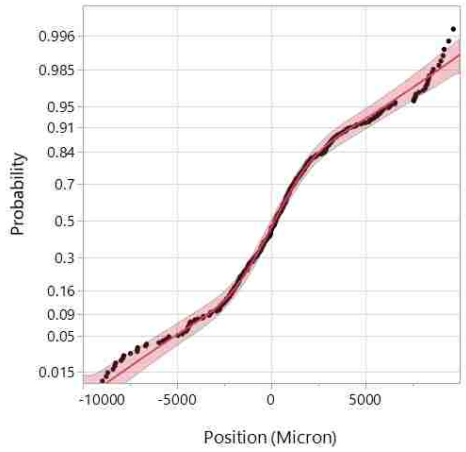

(g) Probability plot of 75-105 µm Al powder

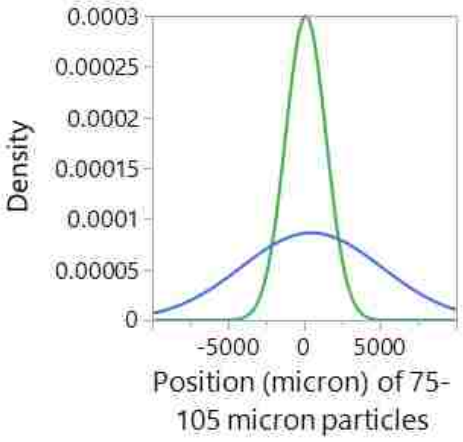

(h) Probability density function for 75-105 µm Al powder

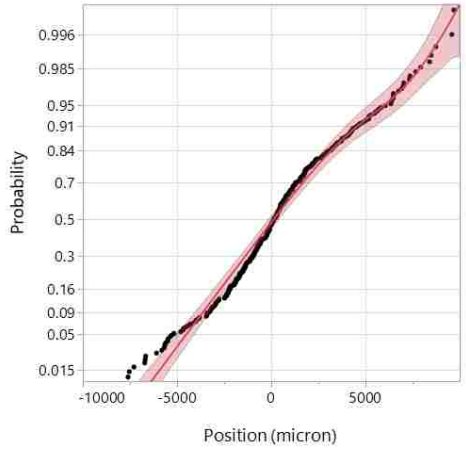

(i) Probability plot of 105-125 µm Al powder

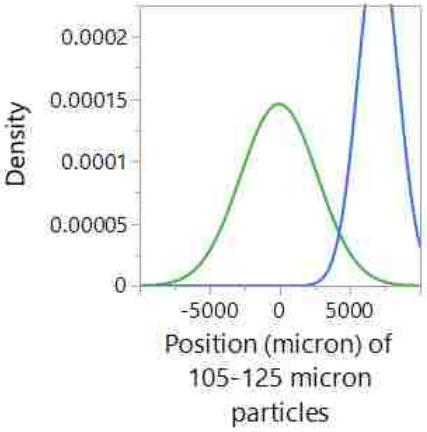

(j) Probability density function for 105-125 µm Al powder

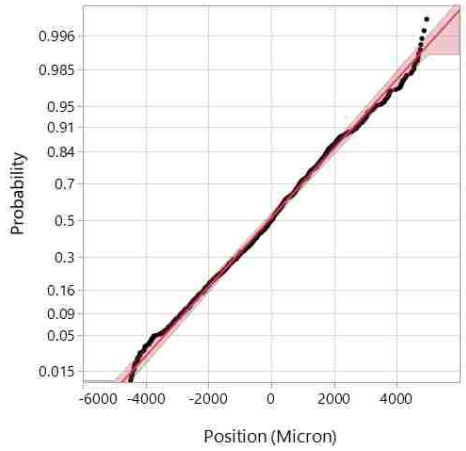

(k) Probability plot of >125 µm Al powder

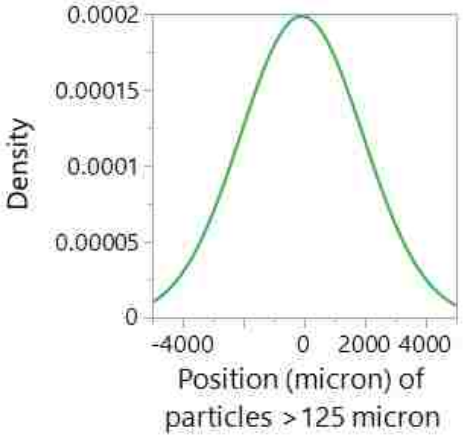

(l) Probability density function for >125 µm Al powder

Figure 3.2. Probability Distribution for Al powder of all size groups (cont.)

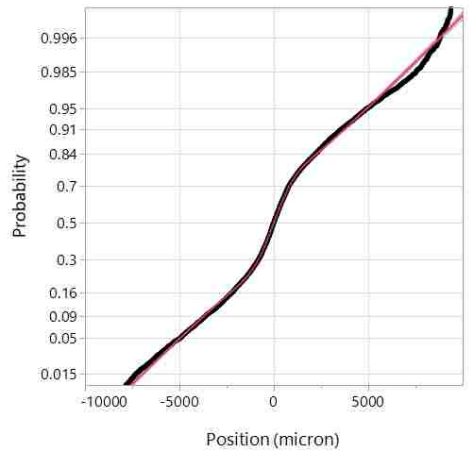

(a) Probability plot of un-sieved V powder

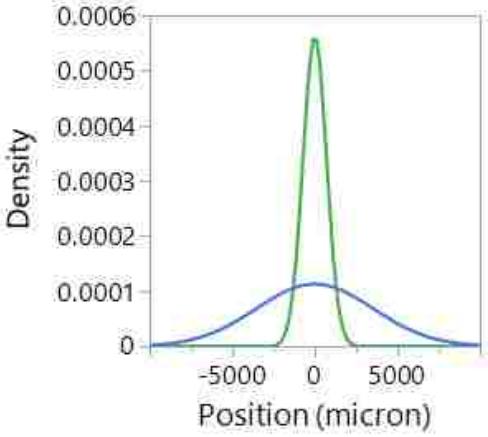

(b) Probability density function for un-sieved V powder

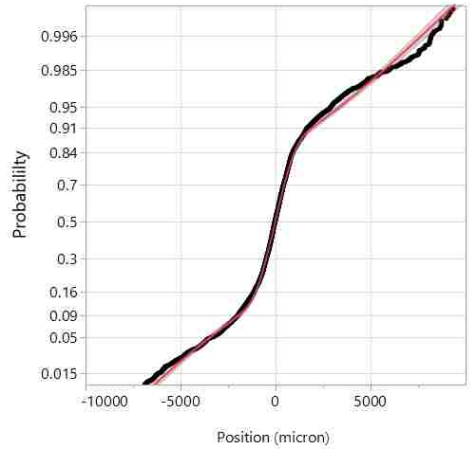

(c) Probability plot of 0-45 µm V powder

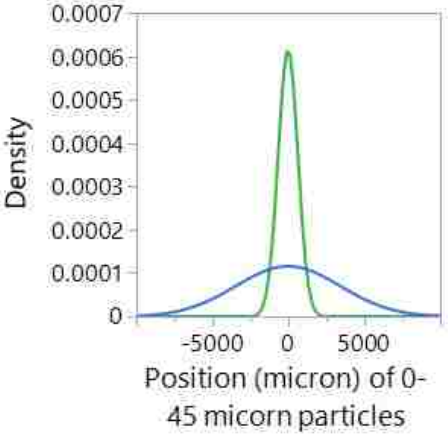

(d) Probability density function for 0-45 µm V powder

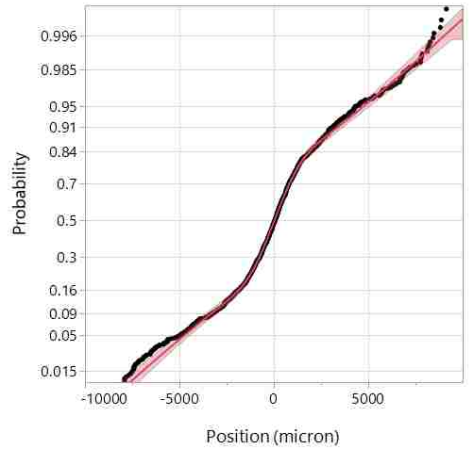

(e) Probability plot of 45-75 µm V powder

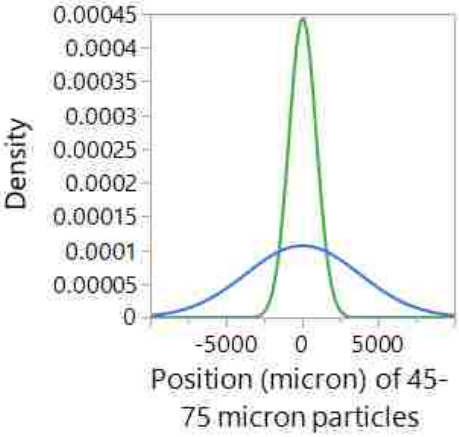

(f) Probability density function for 45-75 µm V powder

Figure 3.3. Probability Distribution for V powder of all size groups

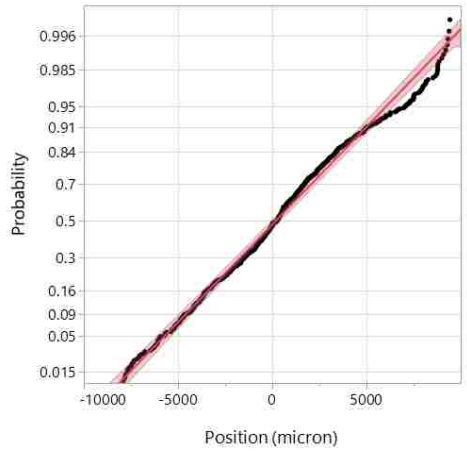

(g) Probability plot of 75-105 µm V powder

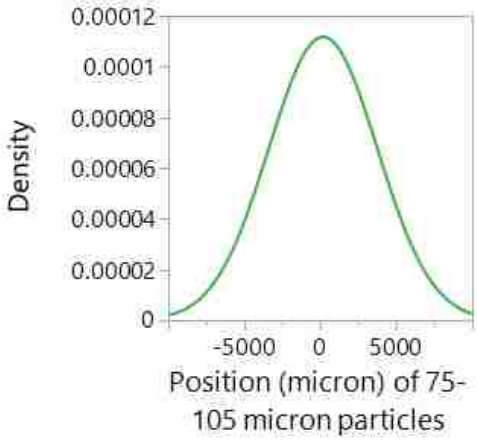

(h) Probability density function for 75-105 µm V powder

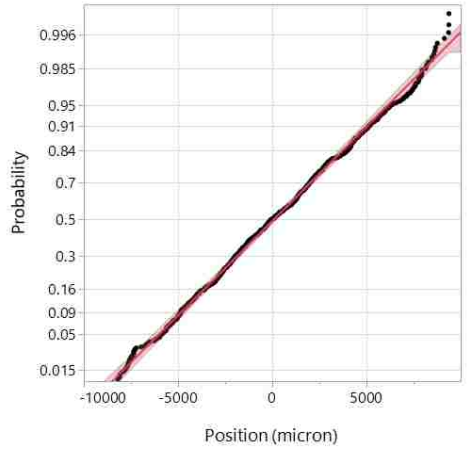

(i) Probability plot of 105-125 µm V powder

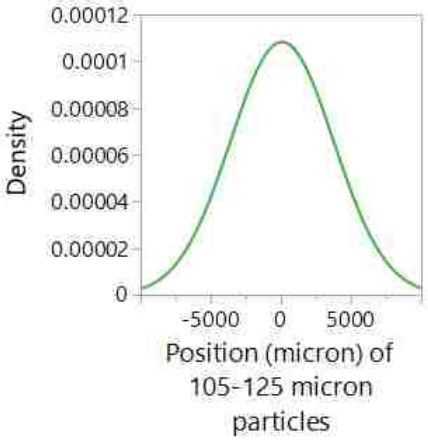

(j) Probability density function for 105-125 µm V powder

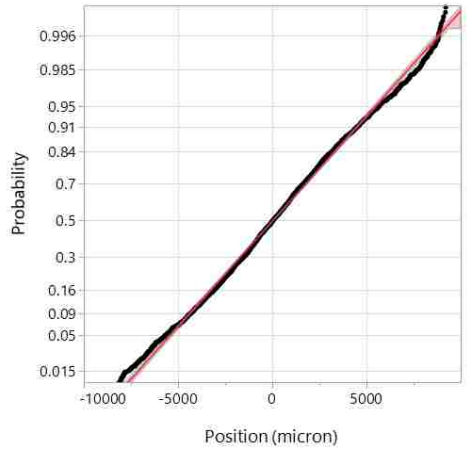

(k) Probability plot of >125 µm V powder

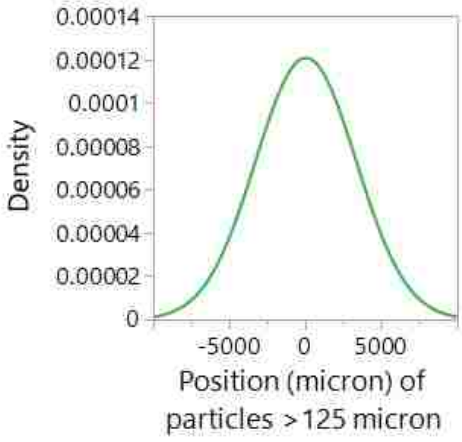

(l) Probability density function for >125 µm V powder

Figure 3.3. Probability Distribution for V powder of all size groups (cont.)

Therefore, the designed volume of elemental powder (V_d) and the powder volume in the melt pool (V_m) have the relationship of $V_d = V_m/R$. In this way, the deposition experiment was conducted by using a mixture of 105-125 μm Ti, 105-125 μm Al, and 105-125 μm V powder with volume percentage ratio of 90.45: 6.82: 2.73 as feedstock to obtain target Ti-6Al-4V material. The deposition experiment design is listed in Table 3.2.

Table 3.1. Probability distribution data of Ti, Al, and V powder

Powder	**Powder Groups**	**Portion 1**	**Standard derivation (σ_1) (μm)**	**Portion 2**	**Standard derivation (σ_2) (μm)**	**Powder probability within 2mm range**
Ti	Un-sieved powder	1	4084.782	0		0.193862
	0-45 μm	1	3883.987	0		0.203182
	45-75 μm	1	3935.994	0		0.200555
	75-105 μm	1	4021.421	0		0.196383
	105-125 μm	1	4075.636	0		0.193823
	>125 μm	1	4182.577	0		0.188962
Al	Un-sieved powder	0.527	1014.006	0.473	4304.115	0.443131
	0-45 μm	0.6201	661.459	0.3799	4944.8404	0.60001
	45-75 μm	0.614	932.266	0.386	4644.998	0.505772
	75-105 μm	0.5662	1328.4508	0.4338	4624.4688	0.384773
	105-125 μm	1	2731.139	0		0.285745
	>125 μm	1	2009.478	0		0.381263
V	Un-sieved powder	0.385	710.156	0.615	3536.683	0.460669
	0-45 μm	0.689	648.226	0.311	3440.817	0.675429
	45-75 μm	0.5145	897.1673	04855	3745.6058	0.480356
	75-105 μm	1	3569.8545	0		0.220617
	105-125 μm	1	3684.3626	0		0.21393
	>125 μm	1	3306.7101	0		0.237665

Table 3.2. Elemental powder percentage ratio in deposition experiment.

powder	Density (kg/m^3)	Size group(μm)	Volume in melt pool	Powder capture rate (R)	Designed Volume
Ti	4507	105-125	20	0.194	90.45
Al	2700	105-125	2.22	0.286	6.82
V	6110	105-125	0.67	0.214	2.73

3.2.MICROSTRUCTURE

Figure 3.4. shows the etched microstructure of deposited Ti-6Al-4V obtained by deposition experiment under an optical microscope. The optical microscope images captured from the different parts in the deposit (Figure 3.4. (a) to (b)) contained lamellar (α+β) basketwave and martensite microstructure respectively.

In Figure 3.4. (a), the darker features were α laths and the brighter features were β ribs. High cooling rates resulted in the formation of a basketweave microstructure. Figure 3.4. (b) showed a mixture of α+β phases and β phase was evenly distributed in the α matrix. It revealed an acicular martensitic microstructure. In the deposit, the Widmanstätten Basketwave is the main type of microstructure that could be found. It tends to form with an increasing cooling rate from the β-phase field [11]. The growth direction of the columnar grains was identified to be along the height of the deposit. This characteristic was expected to be caused by the directional cooling of the LMD process. Analyses of its microstructures revealed that the smaller grain sizes were achieved closer to the substrate in the deposit. The reason was the proximity to the substrate, increased the cooling rate, which would lead to a finer microstructure [12]. Therefore, it was concluded that the steady state section tends

to have the lower cooling rate, which would lead to the formation of the coarser microstructure. A steady state could be observed from middle part to top part.

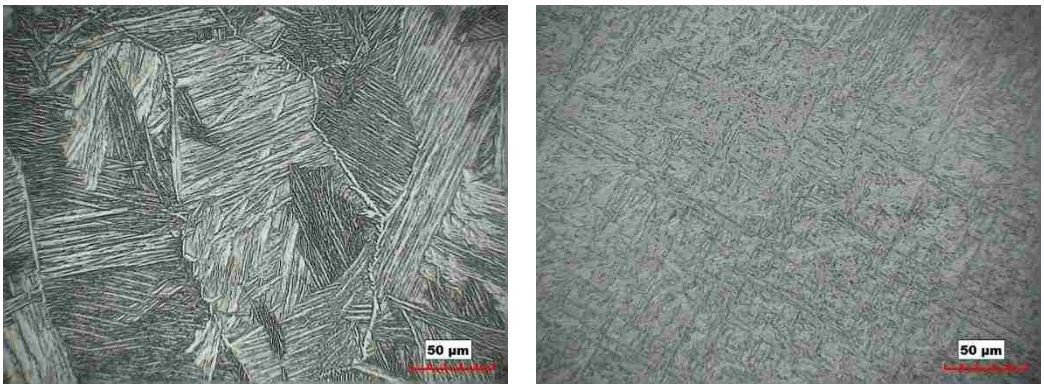

(a) (b)

Figure 3.4. Optical microstructural images of polished and etched deposit

3.3. EDS ANALYSES

EDS chemistry data was gathered from both the standard Ti-6Al-4V and the deposits obtained from deposition experiment. From Table 3.3, it shows that the standard measurement data meet with its certificate of analysis.

Table 3.3. EDS chemistry data gathered from standard Ti64

Element	Standard certificate (wt.%)	Standard measurement (wt.%)
Ti	89.52	89.57
Al	6.36	6.35
V	4.12	4.08

The Ti, Al, and V weight percentage of the deposits are presented in Figure 3.5. As expected, the composition distribution of the deposit obtained by experiment is approximately close to Ti-6Al-4V. The elements weight percentages of all the deposits are within qualified range. It indicates that the alloy is industry qualified Ti64.

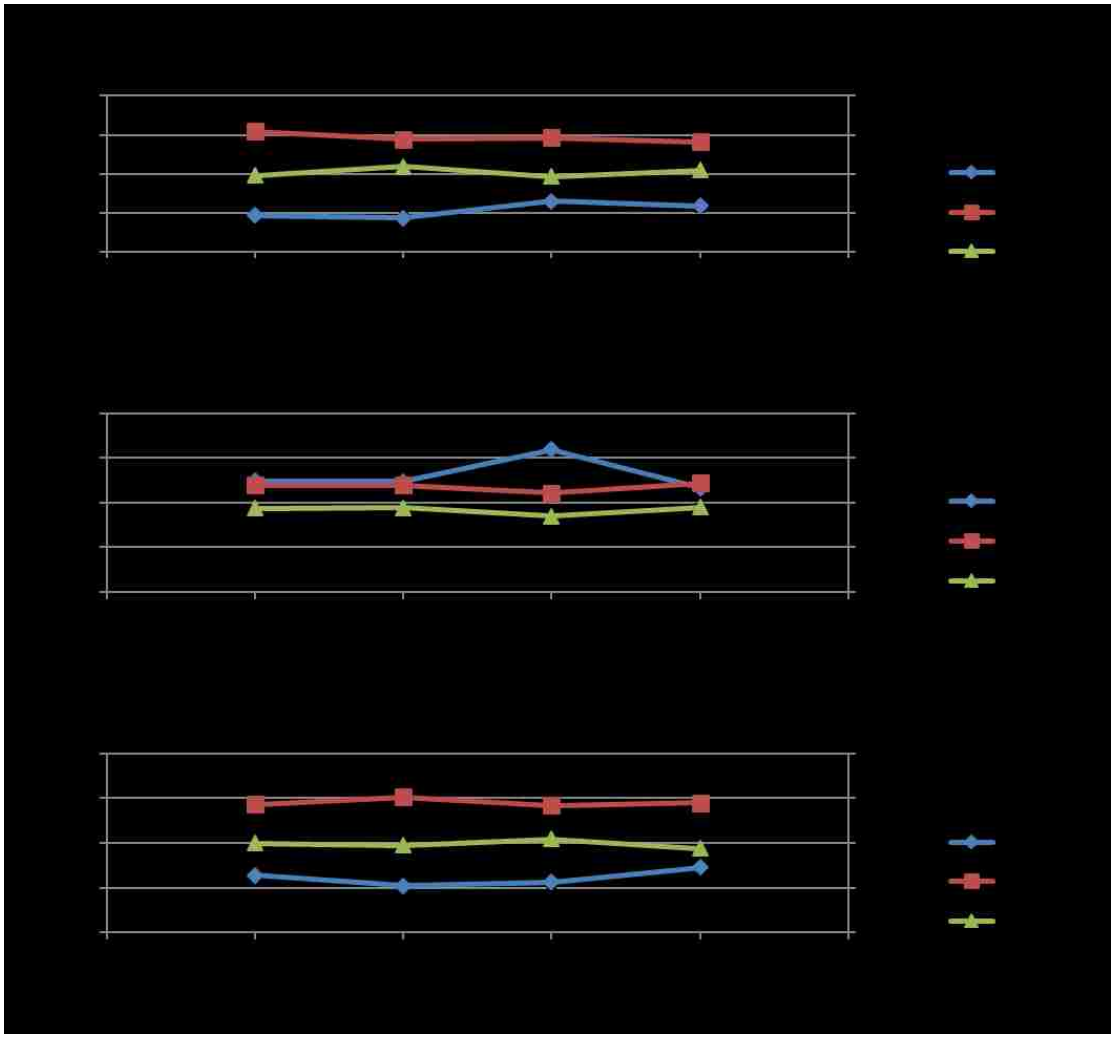

Figure 3.5. Composition distribution along build height direction of the deposits

The EDS line scan data of the deposit was shown in Figure 3.6. It is used to define composition homogeneity. So it seems that the deposit has a homogeneous chemistry distribution along the building height direction. The calculated average composition along the line scan distance is tabulated in Table 3.4. And it shows that their average weight percentage is pretty close to exact Ti64. It appears clearly that the particle distribution of each elemental powder in the mixture is a key factor for the acquired composition in the final deposit. According to the analyses of elemental powder distributions, the qualified Ti-6Al-4V can be easily obtained.

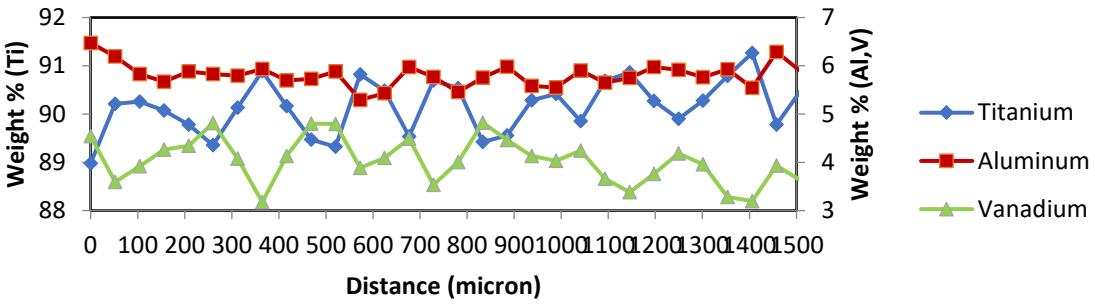

Figure 3.6. EDS line scan along build height direction of the deposit

Table 3.4. Average chemical compositions of elements for the deposited sample

Element	Average wt.%	Wt.% σ
Ti	90.23	0.14
Al	5.78	0.06
V	3.99	0.14

3.4. VICKERS HARDNESS ANALYSIS

The hardness distribution curves of the deposits from deposition experiment is shown in Figure 3.7. The hardness values were taken along the height of the deposit. Indentations were gathered from the Ti-6Al-4V substrate and continued into the deposited parts. Figure 3.7. depicts that the highest hardness values for deposit were observed around the heat affected zones of the deposit. The maximum hardness value of the deposit was around 490 HV. According to the result, the average hardness of the deposits was around 446 HV. It was observed that the Vickers hardness values decreased with progress into the heat affected zone (HAZ) from the substrate side and there was an increase for the first several layers of the deposit zone, then get stabilized beyond that. These values of the deposits are higher than the substrate hardness. This can be attributed to the effect of rapid cooling during the LMD process. It would cause finer microstructure and result in good material properties. Higher values of hardness correlate with higher strengths and wear resistance. Therefore, the deposited Ti-6Al-4V has better wear resistant application.

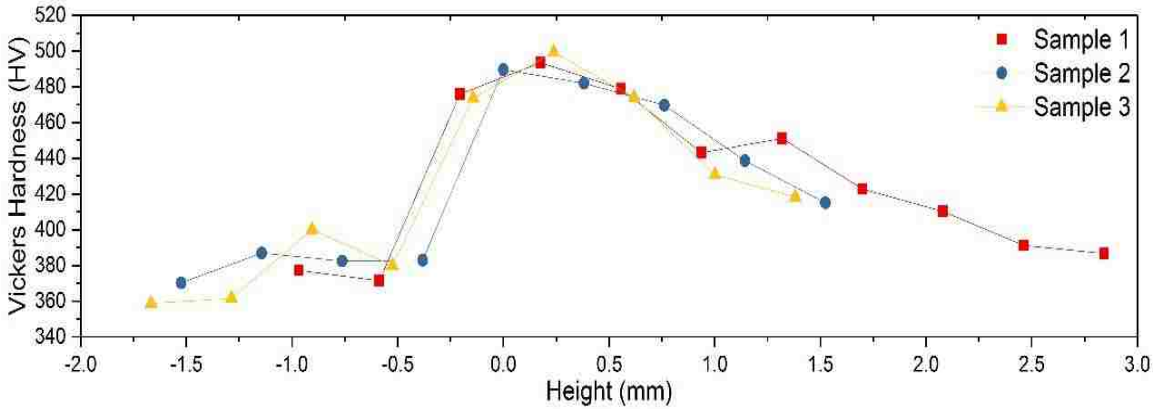

Figure 3.7. The Vickers Hardness results of the deposited alloys

4. CONCLUSIONS

The current research was implemented to investigate the elemental powder effect on composition control for as-deposited parts via the LMD process. By using the suitable condition, the target alloy using elemental powder mixture can be obtained, which ensures the analyses of the elemental powder distributions. The fabricated Ti-6Al-4V alloy from Ti, Al, and V powder mixture was characterized using techniques such as optical microscopy, electron microscopy, hardness testing. It proves that the industry qualified Ti-6Al-4V alloy could be obtained by using elemental powder mixture with designed proportions. Furthermore, this method can be used for fabrication of other alloys by using elemental powder mixture.

REFERENCES

[1] C. Leyens and M. Peters, *Titanium an Titanium Alloys*. 2003.

[2] A. Mahboubi Soufiani, M. H. Enayati, and F. Karimzadeh, “Fabrication and characterization of nanostructured Ti6Al4V powder from machining scraps,” *Adv. Powder Technol.*, vol. 21, no. 3, pp. 336–340, 2010.

[3] C. Qiu, G. A. Ravi, C. Dance, A. Ranson, S. Dilworth, and M. M. Attallah, “Fabrication of large Ti-6Al-4V structures by direct laser deposition,” *J. Alloys Compd.*, vol. 629, pp. 351–361, 2015.

[4] X. Li, C. Wang, W. Zhang, and Y. Li, “Fabrication and characterization of porous Ti6Al4V parts for biomedical applications using electron beam melting process,” *Mater. Lett.*, vol. 63, no. 3–4, pp. 403–405, 2009.

[5] R. Ramakrishnaiah *et al.*, “Preliminary fabrication and characterization of electron beam melted Ti-6Al-4V customized dental implant,” *Saudi J. Biol. Sci.*, 2016.

[6] W. Van Grunsven, E. Hernandez-Nava, G. C. Reilly, and R. Goodall, “Fabrication and Mechanical Characterisation of Titanium Lattices with Graded Porosity,” *Metals (Basel).*, vol. 4, pp. 401–409, 2014.

[7] B. Baufeld, O. Van der Biest, and R. Gault, “Additive manufacturing of Ti-6Al-4V components by shaped metal deposition: Microstructure and mechanical properties,” *Mater. Des.*, vol. 31, no. SUPPL. 1, pp. S106–S111, 2010.

[8] B. Ye, M. R. Matsen, and D. C. Dunand, “Blended elemental powder densification of Ti-6Al-4V by hot pressing,” *J. Mater. Res.*, vol. 26, no. 8, pp. 965–969, 2011.

[9] P. C. Collins, “A combinatorial approach to the development of composition-microstructure-property relationships in titanium alloys using directed laser deposition.” 2004.

[10] X. Chen, L. Yan, W. Li, Z. Wang, F. Liou, and J. Newkirk, “Effect of Powder Particle Size on the Fabrication of Ti-6Al-4V Using Direct Laser Metal Deposition from Elemental Powder Mixture,” vol. 6, pp. 348–355, 2016.

[11] R. Boyer, G. Welsch, and E. W. Collings, *ASM Materials Properties Handbook: Titanium Alloys*. 1994.

[12] M. Simonelli, Y. Y. Tse, and C. Tuck, “Microstructure of Ti-6Al-4V produced by selective laser melting,” *J. Phys. Conf. Ser.*, vol. 371, p. 12084, 2012

III. FABRICATION AND CHARACTERIZATION OF AL$_x$COFENICU$_{1-x}$ HIGH ENTROPY ALLOYS BY LASER METAL DEPOSITION

Xueyang Chen, Lei Yan, Sreekar Karnati, Yunlu Zhang and Frank Liou

Department of Mechanical and Aerospace Engineering

Missouri University of Science and Technology, Rolla, Missouri 65409, U.S.A.

ABSTRACT

High entropy alloys are multicomponent alloys that have at least five different principal elements as alloying elements. Each of these elements has an atomic percentage between 5% and 35%. Typically, they form body-centered cubic (bcc) or face-centered cubic (fcc) structure and are known to possess excellent mechanical properties, corrosion resistance, excellent electric and magnetic properties. Owing to their excellent corrosion and wear resistance, researchers are focusing on employing these materials as coatings. In this research, Laser Metal Deposition (LMD) was used to fabricate $Al_xCoFeNiCu_{1-x}$ (x = 0.25, 0.5, 0.75) high entropy alloys from elemental powder based feedstocks. Thin wall claddings fabricated via LMD were characterized by a variety of techniques. Data from X-ray Diffraction (XRD) and Electron Back Scatter Diffraction (EBSD) suggested that with an increase in Al content and a decrease in Cu content, a change in crystal structure from a predominantly fcc to a combined fcc and bcc structure can be observed. The microstructure of the material was observed to be columnar dendritic. Data from standard less EDS analysis showed that the dendritic phase was Fe and Co enriched while the matrix was Cu and Al enriched in all the considered high entropy alloy fabrications. The Vickers

hardness data was used to estimate the mechanical properties of these deposits. Results also showed that with the increase in aluminum content, $Al_xCoFeNiCu_{1-x}$ displayed higher hardness. The high hardness values imply potential applications in wear resistant coatings.

Keywords: High entropy alloy; Elemental powder; Laser metal deposition

1. INTRODUCTION

High entropy alloys are novel material systems that exhibit properties much more superior than traditional alloys [1]. The high entropy alloys are made up of at least five different principal elements. Typically, these elements have similar atomic size and each element has an atomic composition between 5% and 35% within the alloy. As the name suggests, the mixing of these principal elements causes a large change in entropy. The large change in entropy promotes these elements to solidify into solid solutions instead of forming complex intermetallic compounds. It has been proven that high entropy alloys are capable of excellent mechanical [2,3], electrical, and, magnetic properties [4]. They are also known to have excellent wear resistance [3], corrosion resistance [2,5] and thermal stability [6].

Over the past few years, studies have been conducted over several high entropy alloy systems. Material systems such as, $CoCrCuFeNiTi_x$, $Al_xNbTiMoV$, $CoCrFeMnNiV_x$, $Al_xCoCrCuFeNi$ and $Al_xCoCrFeNi$ have been investigated [7–12]. The fabrication of these materials was performed using production processes such as casting and arc melting. These studies were implemented to systematically study the impact of varying the content of one or more constituent elements on various physical and material properties. Tong et al. [7]

synthesized $Al_xCoCrCuFeNi$ high entropy alloys with different aluminum content by the arc melting and casting methods. They found that variation in Al content can affect the structure of the resultant solid solution phases. Investigations carried out by Wang et al. [8] and Yang et al. [9] on the $Al_xCoCrFeNi$ alloy system also showed that variation in Al caused similar changes in microstructure and mechanical properties. Under the current study, the impact of simultaneously varying Al and Cu content in the $Al_xCoFeNiCu_{1-x}$ system was investigated. Unlike most earlier works involving Al, Co, Cu, Ni and Fe elements, in the current study, Laser Metal Deposition (LMD) was used to fabricate these high entropy materials.

LMD deposition is an additive manufacturing technique capable of fabricating complicated structures with superior properties [13,14]. The applications of this technique include coatings, rapid prototyping, tooling, repair, etc. LMD uses a focused laser beam as a heat source to create a melt pool into which powder feedstock is injected. The powder is metallurgically bonded to the substrate through solidification [15]. The authors theorize that it is particularly beneficial to fabricate high entropy alloys by using LMD, owing to the high melt pool temperature and rapid solidification. The high melt pool temperature can be instrumental in overcoming issues of positive enthalpy of mixing and immiscibility. The high cooling rates produce fine grain size and excellent material properties. These attributes of LMD could potentially ensure fabrication of high entropy alloys with fine and homogenous microstructure.

The main goals of this work involved studying the microstructure and mechanical properties of LMD fabricated $Al_xCoFeNiCu_{1-x}$ high entropy alloys. The impact of simultaneously varying Al and Cu on phase formation and principal crystal structure was

investigated. In this study, 304 Stainless Steel (SS304) was used as the substrate material. The alloy material was fabricated as thin wall claddings and characterized for material properties using optical and Scanning Electron Microscope (SEM) microstructure characterization, hardness testing, X-Ray Diffraction (XRD), Energy Dispersive X-ray Spectroscopy (EDS) and Electron Back Scatter Diffraction (EBSD). The hardness data gathered against SS304 substrates was crucial in assessing the potential application of the alloy system as a wear resistant coating.

2. MATERIALS AND METHODS

2.1. MATERIAL PREPARATION

Under the current study, elemental powders of aluminum, cobalt, iron, nickel, and copper were used as precursor materials. Blends of these powders were made by mixing these elements to achieve different compositions of high entropy alloys. The particle size definitions of Al, Co, Fe, Ni, and Cu powders are listed in Table 2.1.

Table 2.1. Particle size of the original materials

Materials	US Standard Mesh
Co	−100/+325
Fe	−100
Ni	−100/+325
Al	−100
Cu	−325

The chemical compositions of these powders are given in Table 2.2. SS304 was used as the substrate material for these depositions, and substrates were prepared to the dimensions of 2.75 × 2 × 0.25 in.

Table 2.2. Chemical analysis of the original materials (wt.%).

Materials	Fe	C	Ni	Cu	Al	Co	S	Si	Ca	Hydrogen Loss
CO-106	0.002	–	<0.001	<0.0001	–	Bal.	–	–	0.0004	–
FE-103	Bal.	0.003	–	–	–	–	–	–	–	1.01
NI-124	0.01	0.01	Bal.	<0.01	–	0.01	0.02	–	–	–
AL-103	0.07	–	–	–	Bal.	–	–	<0.1	–	–
CU-115	–	–	–	Bal.	–	–	–	–	–	0.28

2.2. DEPOSITION SYSTEM

In this study, a 1 kW continuous wave fiber laser with a wavelength of 1064 nm was used to deposit the elemental powder blends. A melt pool spot size of approximately 2 mm was obtained through a lens of 750 mm focal length. A ceramic tube nozzle was used in conjuncture with a CNC (Computer Numerical Control) table to facilitate movement and perform deposition. Argon gas was used to implement an inert atmosphere and was also used as a carrier gas to deliver the powder mixture to the melt pool.

2.3. EXPERIMENTAL PROCEDURE

Powders were weighed for desired alloy compositions in a glove box under an argon atmosphere and sealed in bottles. The as-blended atomic percentages of these powder mixtures can be represented by $Al_xCoFeNiCu_{1-x}$, where x = 0.25, 0.5, 0.75. These bottles

were then shaken using a Turbula® mixer (Glen Mills Inc., Maywood, NJ, United States) for 20 min to obtain thorough mixing and homogeneity within the powder blends.

A schematic layout of the LMD system is shown in Figure 1. Thin wall claddings were fabricated by performing single melt pool, layer by layer deposition. To ensure perfect bonding, before deposition, a preheat scan was performed by running the laser across the surface of the substrate at 1 kW power and without powder. The preheating process was used to heat up the substrate and rid the surface of the substrate from oxide scale buildup, surface impurities, and, surface imperfections. Laser transverse speed was set at 600 mm/min for all the depositions. The initial 10 layers of deposition carried out a power to 1 kW to ensure perfect bonding with the substrate. The rest of the deposition was carried at a power of 400 W. The same deposition scheme and parameters were used for all the depositions. This was expected to ensure an unbiased comparison between different depositions.

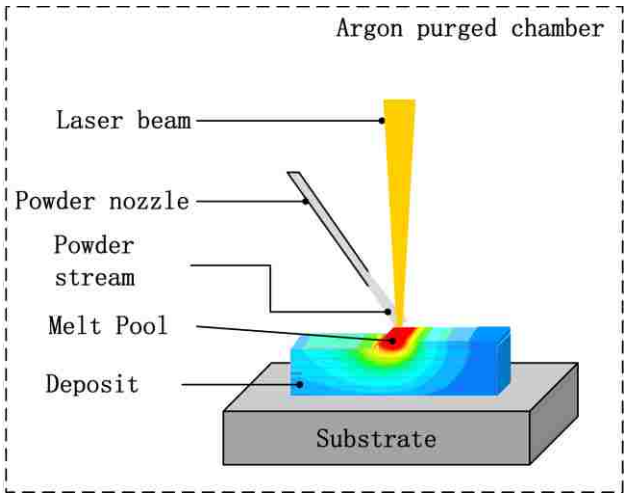

Figure 2.1. Schematic layout of the LMD (Laser Metal Deposition) system [16]

After deposition, vertical transverse sections were cut using a wire Electro-Discharge Machine (wire-EDM, Hansvedt Industries Inc., Rantoul, IL, United States) and mounted in Bakelite for grinding and polishing. Aqua Regia, 30 mL HCl, and 10 mL HNO_3 was used for etching. Hirox optical microscope was used to perform microstructure imaging. Helios Nanolab 600 SEM (FEI Company, Hillsboro, OR, United States) equipped with an Oxford Energy Dispersive Spectrometer and HKL Electron Backscatter Diffraction system was used to get the chemical compositions and crystal structure data. The Vickers hardness measurements were performed on the three different compositions using a Struers Duramin micro-hardness tester(Struers Inc., Cleveland, OH, United States). Press load of 9.81 N and load time of 10 s was used during the hardness tests.

3. RESULTS AND DISCUSSION

3.1. THEORY

The possibility of forming a solid solution can be predicted by the Hume–Rothery rules. Zhang et al. [17,18] have predicted phase formation for the multi-component alloys by calculating parameters Ω and δ. Ω is a parameter that combines effects of ΔS_{mix} and ΔH_{mix} on the stability of the multicomponent solid solution, and it is defined as Equation (1). δ is the mean square deviation of the atomic size of elements. It is used to describe the comprehensive effect of the atomic size difference in multi-element alloys, and the parameter δ is calculated using Equation (2) [19]. These parameters can be used to predict the possibility of solid-solution formation for multi-component alloys. Per Zhang, when $\Omega \geq 1.1$ and $\delta \leq 6.6\%$, a stable solid solution would be obtained post solidification [18]

$$\Omega = \frac{T_{\mathrm{m}}\Delta S_{\mathrm{mix}}}{|\Delta H_{\mathrm{mix}}|} \quad (1)$$

The melting point of *n*-elements alloy, T_{m}, is calculated using the rule of mixtures: $T_{\mathrm{m}} = \sum_{i=1}^{n} c_i (T_{\mathrm{m}})_i$, where $(T_{\mathrm{m}})_i$ is the melting point of the *i*th component of alloy. The enthalpy of mixing, ΔH_{mix}, can be determined by the equation, $\Delta H_{\mathrm{mix}} = \sum_{i=1, i\neq j}^{n} \Omega_{ij} c_i c_j$, where $\Omega_{ij} = 4\Delta H_{ij}^{\mathrm{mix}}$ is the solution interaction parameter between the *i*th and *j*th elements, and c_i and c_j are the mole fractions of the *i*th and *j*th component [20]. The remaining parameter, ΔS_{mix} is the entropy of the mixture. It was calculated by following the Boltzmann's hypotheses, the entropy of mixing of an *n*-element solution is (assuming they are in the liquid or fully solid solution state) $\Delta S_{\mathrm{mix}} = -R \sum_{i=1}^{n} (c_i \ln c_i)$, where c_i is mole fraction of component, $\sum_{i=1}^{n} c_i = 1$, and R =8.314 J/(K·mol) is a gas constant. In Equation (2), n is the number of the components in an alloy system, $\bar{r} = \sum_{i=1}^{n} c_i r_i$ is the average atomic radius, and r_i is the atomic radius of the *i*th component [21]

$$\delta = \sqrt{\sum_{i=1}^{n} c_i (1 - r_i/\bar{r})^2} \quad (2)$$

The characteristic parameters of the elements in the $Al_xCoFeNiCu_{1-x}$ alloys are tabulated in Table 3.1. [21]. The mixing enthalpy ($\Delta H_{ij}^{\mathrm{mix}}$) of binary alloys are listed below in Table 3.2. [22]. According to Equations (1) and (2) and the parameters in Tables 3.1. and 3.2., the values of Ω and δ for the compositions considered in this study were calculated and tabulated in Table 3.3. The values of these parameters for the compositions under

consideration were in range for solid solution formation. It shows that the $Al_xCoFeNiCu_{1-x}$ (x = 0.25, 0.5, 0.75) alloys should have the high entropy effect and should easily form solid solutions. The high entropy effect should inhibit the formation of intermetallic compounds and promote the formation of solution phases. This is expected to reduce the number of phases and cause much simpler microstructures.

Table 3.1. Characteristic parameters of Al, Co, Fe, Ni and Cu element [21]

Elements	**Atomic Number**	**Atomic Radius(Å)**	**Crystal Structure**	**Melting Point (K)**
Al	13	1.43	fcc	933.5
Co	27	1.25	hcp	1770
Fe	26	1.27	bcc	1811
Ni	28	1.25	fcc	1728
Cu	29	1.28	fcc	1358

Table 3.2. The enthalpy of mixing of binary i-j system ($\Delta H_{ij}^{\mathrm{mix}}$) at an equi-atomic composition [22]

***i-j* System**	**$\Delta H_{ij}^{\mathrm{mix}}$ (kJ/mol)**
Al-Co	−19
Al-Fe	−11
Al-Ni	−22
Al-Cu	−1
Co-Fe	−1
Co-Ni	0
Co-Cu	6
Fe-Ni	−2
Fe-Cu	13
Ni-Cu	4

Table 3.3. The values of Ω and δ of the $Al_xCoFeNiCu_{1-x}$ (x = 0.25, 0.5, 0.75) high entropy alloys

Alloys	T_m (K)	ΔH_{mix} (KJ/mol)	ΔS_{mix} (J/(K·mol))	Ω	δ
$Al_{0.25}CoFeNiCu_{0.75}$	1640	0.27	12.7	78.39	3.4%
$Al_{0.5}CoFeNiCu_{0.5}$	1614	−4.44	12.96	4.72	4.5%
$Al_{0.75}CoFeNiCu_{0.25}$	1587	−9.11	12.69	2.21	5.2%

3.2.XRD

XRD tests were used to identify the crystal structure of the deposits. The XRD tests were performed using a XPERT Pro-type diffractometer (PANalytical, Almelo, Netherlands) with Cu as the anode material. The XRD patterns from the $Al_xCoFeNiCu_{1-x}$ (x = 0.25, 0.5, 0.75) deposits are shown in Figure 3.1. In this figure, the dot (•) is used to represent FCC peak pattern, and clubs (♣) represent the BCC peak pattern. The peak patterns of FCC solid solution were observed in $Al_{0.25}CoFeNiCu_{0.75}$ and $Al_{0.5}CoFeNiCu_{0.5}$, while both FCC and BCC structures were present in the $Al_{0.75}CoFeNiCu_{0.25}$ alloy. The XRD pattern of the $Al_{0.5}CoFeNiCu_{0.5}$ was similar to that of $Al_{0.25}CoFeNiCu_{0.75}$. A leftward i.e., lower 2-theta peak shift was seen from $Al_{0.25}CoFeNiCu_{0.75}$ to $Al_{0.5}CoFeNiCu_{0.5}$. This shift can be attributed to a decrease in copper content. The estimated values of the lattice parameters for FCC structure were also seen to increase with increasing Al content (Table 3.4.).

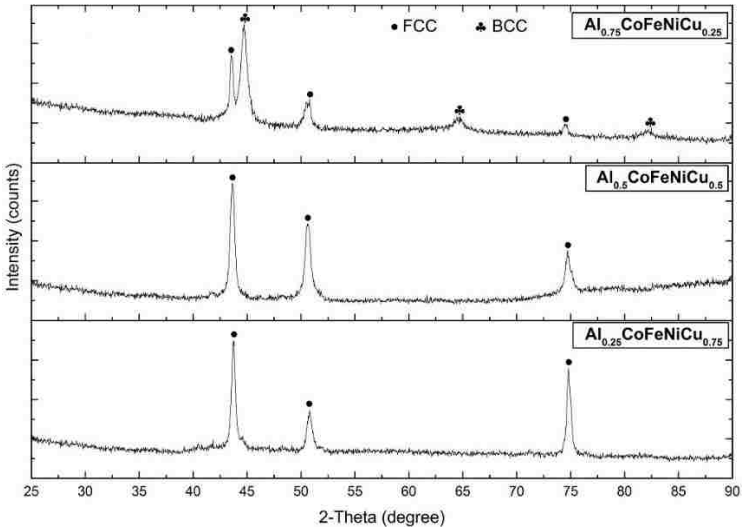

Figure 3.1. The XRD patterns of the AlxCoFeNiCu1−x (x = 0.75, 0.5, 0.25) alloys, dot (•) represents the fcc peak pattern, and clubs (♣) represents the bcc peak pattern.

From Figure 3.1., the increase in aluminum and decrease in copper, in $Al_{0.25}CoFeNiCu_{0.75}$ to $Al_{0.75}CoFeNiCu_{0.25}$, resulted in a change from complete fcc structure to a combined fcc and bcc structure. Therefore, it can be said that Cu promotes fcc phase formation while Al promotes bcc phase formation. However, it is the author's belief that, between aluminum and copper, aluminum has a larger impact on causing the change in crystal structure. A substitutional solid solution is possible between elements of the similar atomic radius. Among the five constituent elements, aluminum has the largest atomic radius [23]. At lower percentages of aluminum, the substitutional solid solution is expected to be feasible. However, aluminum still causes distortion in the lattice structure owing to its larger atomic size [24]. Therefore, at larger percentages of aluminum, a bcc phase would be promoted over a substitutional fcc solid solution.

Table 3.4. Lattice parameters in the $Al_xCoFeNiCu_{1-x}$ (x = 0.25, 0.5, 0.75) alloys

Alloy	Phase Name	Lattice Parameter (Å)
$Al_{0.25}CoFeNiCu_{0.75}$	fcc	3.5882
$Al_{0.5}CoFeNiCu_{0.5}$	fcc	3.5920
$Al_{0.75}CoFeNiCu_{0.25}$	fcc	3.6007
	bcc	2.8724

3.3. MICROSTRUCTURE

Images of transverse sections of the deposit and the substrate obtained from all the three powder mixtures are shown in Figure 3.2. A minimum of 6 mm height was deposited using each powder mixture.

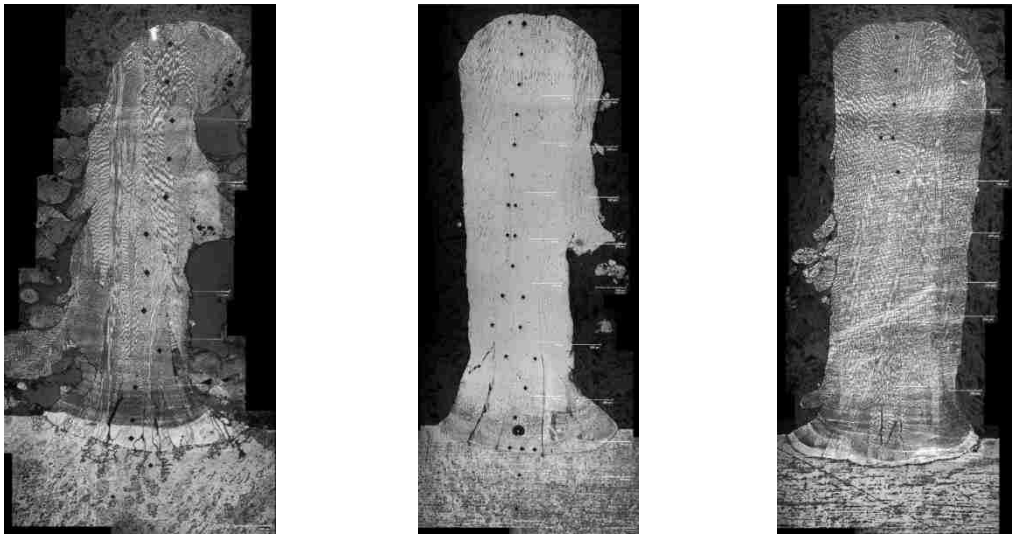

(**a**) (**b**) (**c**)

Figure 3.2. Optical microstructural images of polished and etched transverse sections of all the $Al_xCoFeNiCu_{1-x}$ (x = 0.25, 0.5, 0.75) high entropy alloy deposits. (a) Transverse section of the $Al_{0.25}CoFeNiCu_{0.75}$ alloy and SS304 substrate; (b) Transverse section of the Al0.5CoFeNiCu0.5 alloy and SS304 substrate; (c) Transverse section of the Al0.75CoFeNiCu0.25 alloy and SS304 substrate

Figure 3.3. (a)–(c) shows the etched microstructures of $Al_xCoFeNiCu_{1-x}$ (x = 0.25, 0.5, 0.75) high entropy alloys captured under an optical microscope.

(**a**)

(**b**)

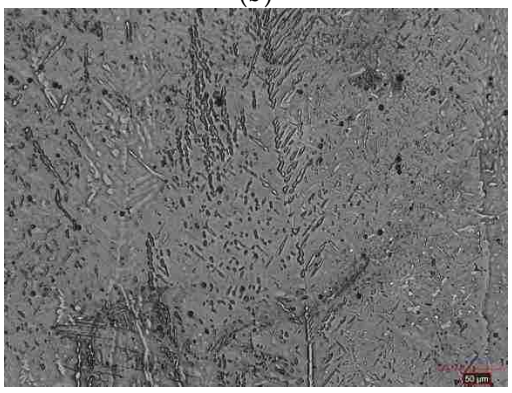

(**c**)

Figure 3.3. Images reveal a columnar dendritic microstructure in all the $Al_xCoFeNiCu_{1-x}$ (x = 0.25, 0.5, 0.75) high entropy alloy deposits. (a) $Al_{0.25}CoFeNiCu_{0.75}$; (b) $Al_{0.5}CoFeNiCu_{0.5}$; (c) $Al_{0.75}CoFeNiCu_{0.25}$

The etched microstructure of $Al_{0.25}CoFeNiCu_{0.75}$ was composed of columnar dendritic material. The growth direction of these columnar grains was identified to be along the height of the deposit. This characteristic was expected to be caused by the directional cooling of the LMD process. The $Al_{0.5}CoFeNiCu_{0.5}$ deposit also had columnar dendritic material. The etched microstructure of $Al_{0.75}CoFeNiCu_{0.25}$ depicts a dendritic microstructure as well. Coarsening of the microstructure can be observed by comparing the dendrites of $Al_{0.25}CoFeNiCu_{0.75}$ and $Al_{0.5}CoFeNiCu_{0.5}$. This change can be attributed to the drop in the solidus–liquidus temperature caused by the addition of aluminum (Table 3.3). Since the power parameters stayed the same for all of the deposits, a decrease in solidus–liquidus temperatures would increase the super heat in the melt pool and would thereby cause a slower cooling rate.

3.4. EBSD AND EDS ANALYSES

In the aim of further differentiating structure and phase information of the $Al_xCoFeNiCu_{1-x}$ (x = 0.25, 0.5, 0.75) alloys, EBSD and EDS measurements were performed. Regions of interest and the phase analyses of $Al_{0.25}CoFeNiCu_{0.75}$, $Al_{0.5}CoFeNiCu_{0.5}$ and $Al_{0.75}CoFeNiCu_{0.25}$ alloys are shown in Figures 3.4. – 3.6., respectively. Figures 3.4. and 3.5. conclude an fcc crystal structure in the $Al_xCoFeNiCu_{1-x}$ (x = 0.25, 0.5) fabrications. $Al_{0.75}CoFeNiCu_{0.25}$, however, contained both fcc and bcc phases. The phase fractions of fcc and bcc phases for the $Al_xCoFeNiCu_{1-x}$ (x = 0.25, 0.5, 0.75) deposits were as listed in Table 3.5. These results agreed with the conclusions from XRD analysis.

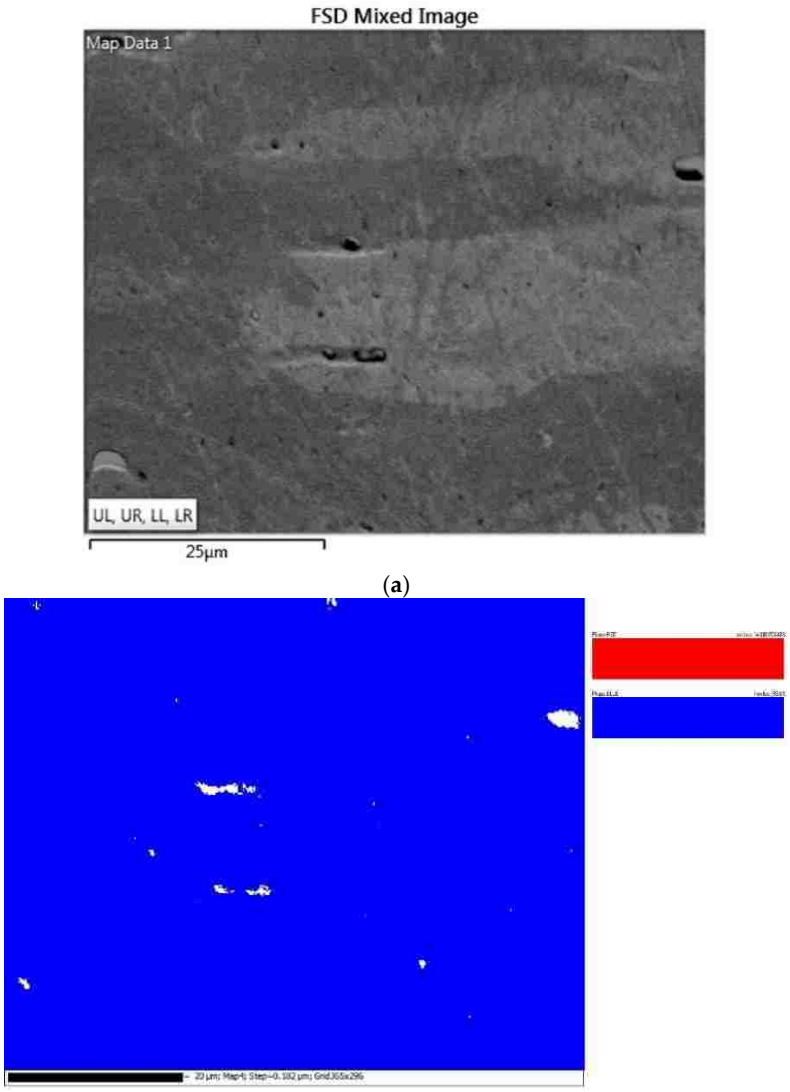

(**a**)

(**b**)

Figure 3.4. EBSD phase map indicating predominantly fcc phase in the $Al_{0.25}CoFeNiCu_{0.75}$ fabrication. (a) Region of interest on $Al_{0.25}CoFeNiCu_{0.75}$; bright and dark phases represent two grains of different orientation; (b) Phase map showing predominantly fcc phase (represented by blue color) within the region of interest

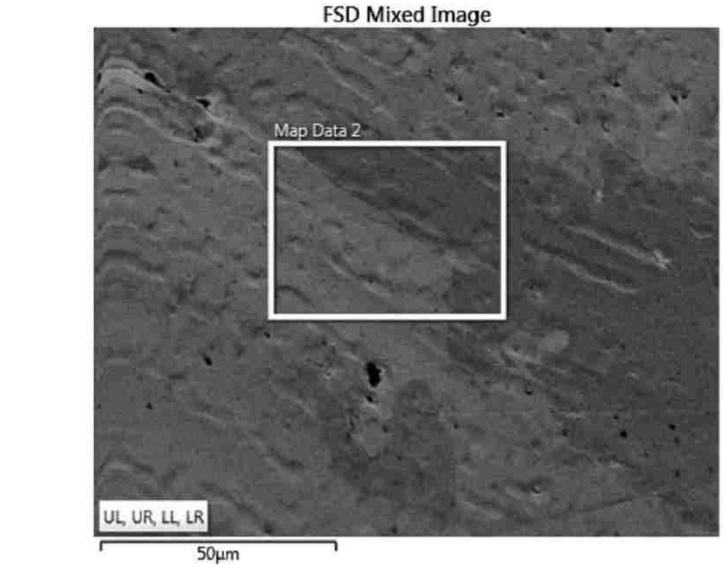

(**a**)

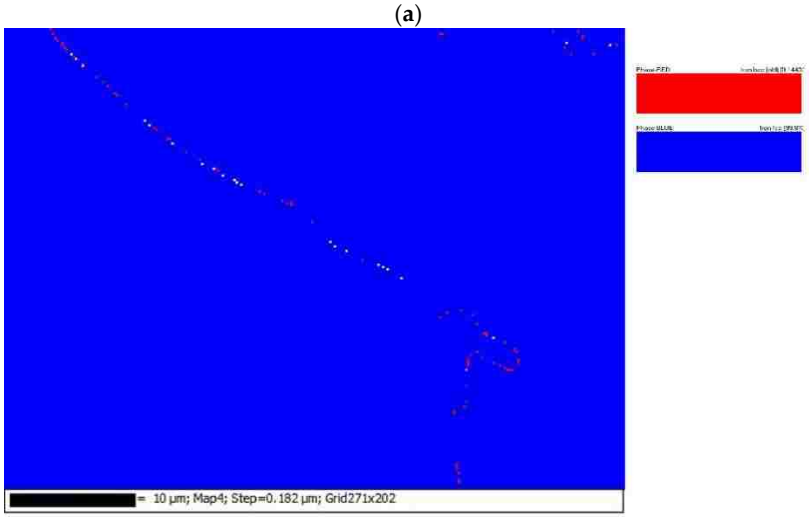

(**b**)

Figure 3.5. EBSD phase map indicating predominantly fcc phase in the $Al_{0.5}CoFeNiCu_{0.5}$ fabrication. (a) Region of interest (enclosed within the white rectangle) on Al0.5CoFeNiCu0.5, bright and dark phases represent two grains of different orientation; (b) Phase map indicating mostly fcc phase (represented by blue color) in the region of interest

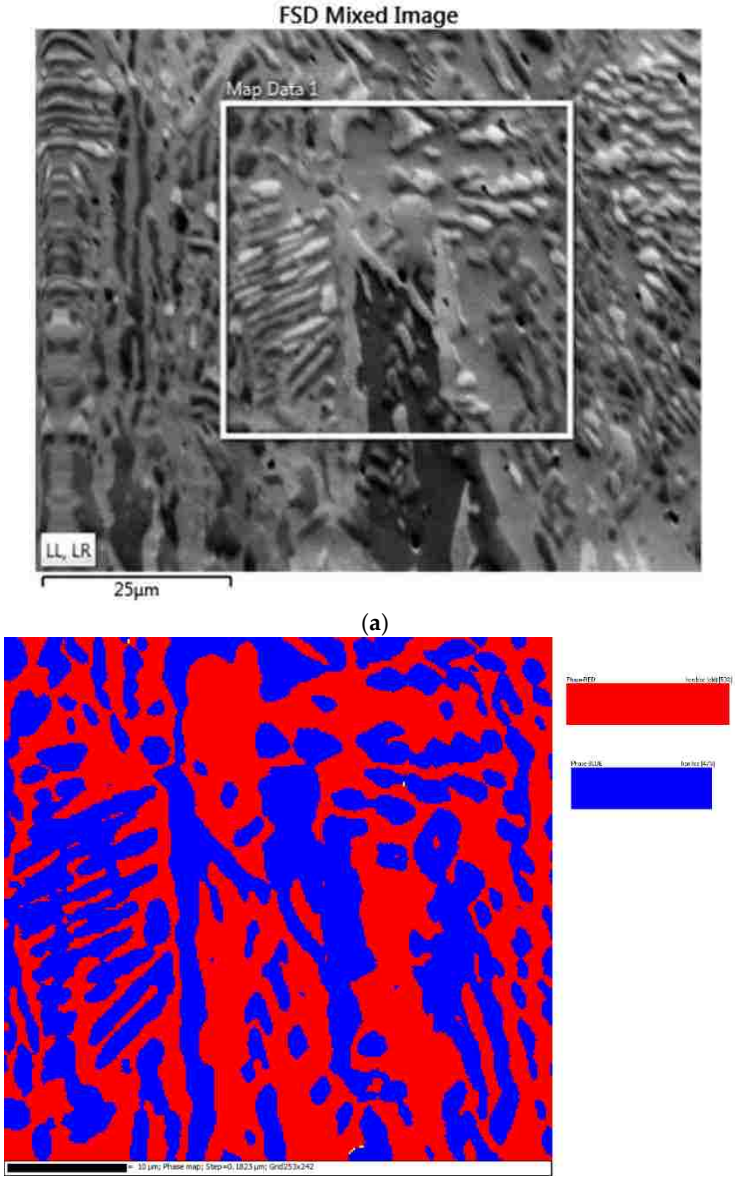

(**a**)

(**b**)

Figure 3.6. EBSD phase map indicating both fcc and bcc phases in the $Al_{0.75}CoFeNiCu_{0.25}$ fabrication. (a) Region of interest (enclosed within the white rectangle) on Al0.75CoFeNiCu0.25, bright and dark phases represent two grains of different orientation; (b) Phase map indicating fcc phase (represented by blue color) and bcc phase (represented by red color) in the region of interest

Table 3.5. Phase fractions of fcc and bcc phases in the region of interest for the $Al_xCoFeNiCu_{1-x}$ (x = 0.25, 0.5, 0.75) fabrications

$Al_xCoFeNiCu_{1-x}$ (x = 0.25, 0.5, 0.75)	**Phase Name**	**Phase Fraction (%)**
$Al_{0.25}CoFeNiCu_{0.75}$	bcc	0.01
	fcc	99.56
	Zero Solution	0.44
$Al_{0.5}CoFeNiCu_{0.5}$	bcc	0.14
	fcc	99.81
	Zero Solution	0.04
$Al_{0.75}CoFeNiCu_{0.25}$	bcc	52.62
	fcc	46.42
	Zero Solution	0.96

Figures 3.7. – 3.9. show the EDS elemental maps obtained from the $Al_xCoFeNiCu_{1-x}$ (x = 0.25, 0.5, 0.75) fabrications. The same regions of interest considered in Figures 3.4. – 3.6. were used for this EDS analysis. The Fe-Kα, Al-Kα, Ni-Kα, Co-Kα, and Cu-Kα signals were used to estimate the elemental distributions within the regions of interest. Figure 3.7. indicates that the $Al_{0.25}CoFeNiCu_{0.75}$ fabrication contained predominantly two phases. The dendritic phase (also seen in Figure 3.3. (a)) was observed to be Cu and Al deficient, whereas the matrix was Cu and Al rich. The authors theorize that the positive enthalpy of mixing between Cu-Ni, Cu-Fe, and Cu-Co is expected to create segregation. This separation persists in the microstructure due to the rapid solidification of LMD process. The Cu and Al deficient fraction having higher proportions of Fe, Co, and Ni would have higher solidus–liquidus temperatures. Therefore, this fraction of the melt pool would solidify first to form the dendritic phase. The matrix being Cu and Al rich would have lower solidus–liquidus temperature values and would, therefore, solidify last. Figure 3.8. indicates that the $Al_{0.5}CoFeNiCu_{0.5}$ fabrication also contained predominantly two phases. Like $Al_{0.25}CoFeNiCu_{0.75}$, the dendritic phase (also seen in Figure 3.3. (b)) was observed to be Cu and Al deficient, whereas the matrix was Cu and Al rich. However,

nickel was observed to be more homogenously distributed in the $Al_{0.5}CoFeNiCu_{0.5}$ fabrication. This could be attributed to the increase in Al content and the highly negative enthalpy of mixing between Al and Ni. This increase in Al content can also be visualized from the increase in signal in the Al elemental map. From Figure 3.9., the acquired elemental maps show that the $Al_{0.75}CoFeNiCu_{0.25}$ alloy was composed of the Fe/Co-rich dendritic phase and Ni/Al-rich matrix. The negative enthalpy of mixing between Al and Ni is expected to cause the Ni enrichment in the matrix. Al was expected to promote bcc phase formation, the EDS elemental map data and the EBSD phase map data have been observed to be in support of this statement. The dendritic phase contained an fcc crystal structure (Al deficient) and the matrix contained a bcc structure (Al rich).

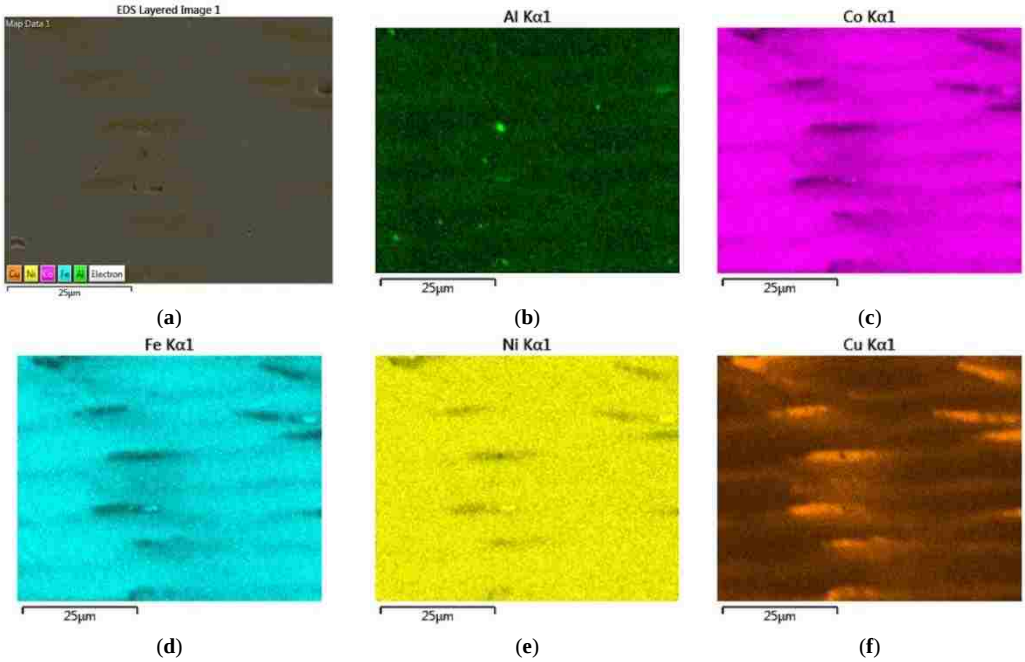

Figure 3.7. EDS elemental maps of $Al_{0.25}CoFeNiCu_{0.75}$ alloy from the region of interest shown in Figure 3.4. (a). (a) EDS layered image; (b) Element map of Al; (c) Element map of Co; (d) Element map of Fe; (e) Element map of Ni; (f) Element map of Cu

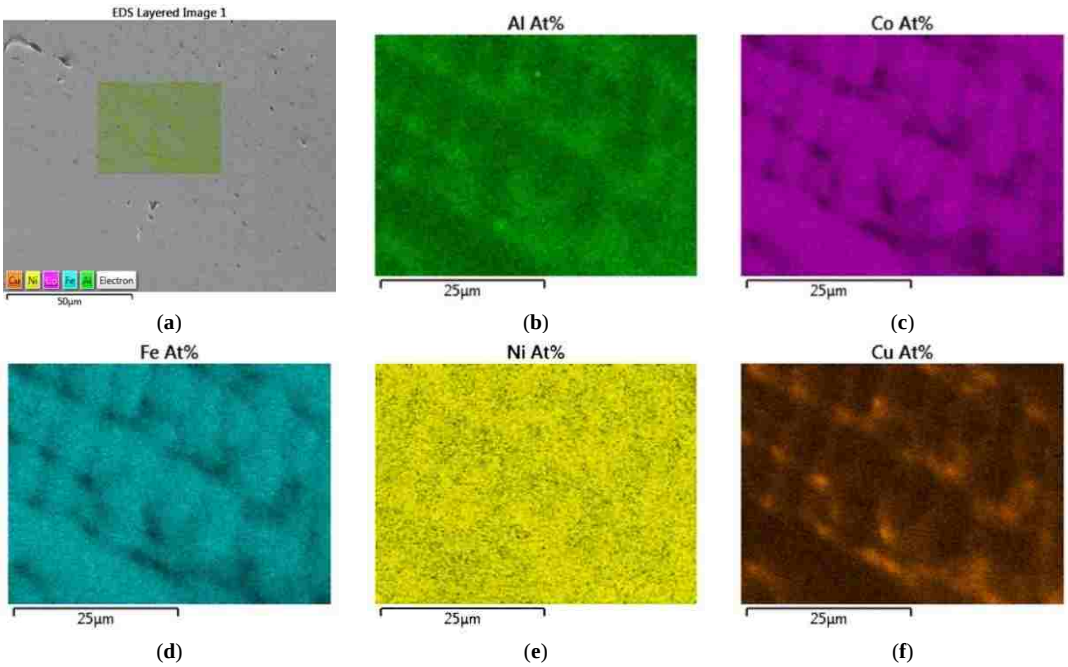

Figure 3.8. EDS elemental maps of $Al_{0.5}CoFeNiCu_{0.5}$ alloy from the region of interest shown in Figure 3.5. (a). (a) EDS layered image; (b) Element map of Al; (c) Element map of Co; (d) Element map of Fe; (e) Element map of Ni; (f) Element map of Cu

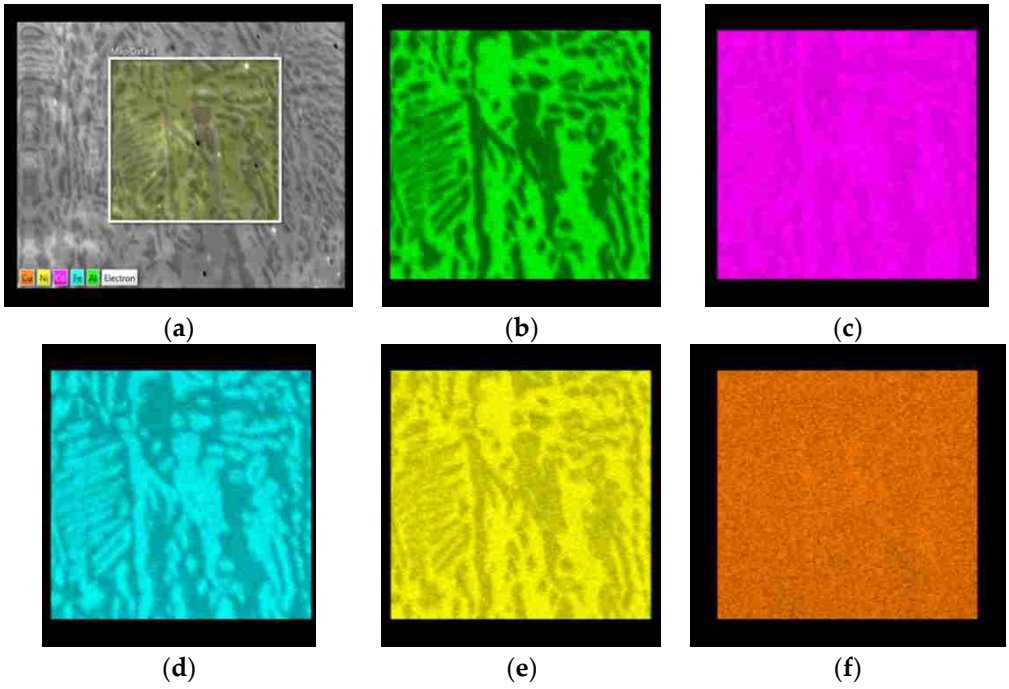

Figure 3.9. EDS elemental maps of $Al_{0.75}CoFeNiCu_{0.25}$ alloy from the region of interest shown in Figure 3.6. (a). (a) EDS layered image; (b) Element map of Al; (c) Element map of Co; (d) Element map of Fe; (e) Element map of Ni; (f) Element map of Cu

EDS chemistry data was gathered from the dendritic and matrix phases in the microstructures of different alloy compositions. The standard less measurements form the phases and grains (bright and dark regions captured in the FSD (Forward Scatter Detector) mixed images shown in Figures 3.4. (a), 3.5. (a), and 3.6. (a)) are shown in Table 3.6. The variation observed from the elemental maps is again noticed from the values of the atomic composition. Minimal variation in chemistry was noticed between the grains seen in the FSD images. The as-blended composition and average composition calculated from each grain were very close for all elements expect for the case of aluminum. This difference could be attributed to the loss of aluminum during transport to the melt pool (Al powder is comparatively very light in weight) and evaporation due to the lower melting and boiling points.

Table 3.6. Chemical composition of the elements at different regions in atomic % for the $Al_xCoFeNiCu_{1-x}$ (x = 0.25, 0.5, 0.75) alloys

Alloy	Area	Al	Fe	Co	Ni	Cu
$Al_{0.25}CoFeNiCu_{0.75}$	As-blended composition	6.25	25	25	25	18.75
	Bright phase (Figure 5a)	4.47	26.85	22.15	28.08	18.45
	Dark phase (Figure 5a)	4.27	27.8	23.2	28.47	16.26
	Dendrite (FCC)	4.32	27.84	23.23	28.41	16.2
	Matrix (FCC)	5.05	16.19	12.78	23	42.98
$Al_{0.5}CoFeNiCu_{0.5}$	As blended composition	12.5	25	25	25	12.5
	Bright phase (Figure 6a)	9.21	25.57	26.44	27.54	11.24
	Dark phase (Figure 6a)	9.94	23.7	24.7	28.23	13.43
	Dendrite (FCC)	9.3	25.03	26	28	11.67
	Matrix (FCC)	11.72	17.65	18.93	28	23.7
$Al_{0.75}CoFeNiCu_{0.25}$	As blended composition	18.75	25	25	25	6.25
	Bright phase (Figure 7a)	20.39	23.7	18.92	30.63	6.36
	Dark phase (Figure 7a)	21.42	22.86	18.22	31.19	6.31
	Dendrite (FCC)	9.85	35.58	22.06	25.53	6.98
	Matrix (BCC)	21.19	22.43	19.1	31.22	6.06

3.5. VICKERS HARDNESS ANALYSIS

The hardness distribution curves of $Al_xCoFeNiCu_{1-x}$ (x = 0.25, 0.5, 0.75) high entropy alloys samples are shown in Figure 3.10. The hardness curves were gathered along the height of the deposit. Indentations were gathered from the substrate SS304 and continued into the deposit. A fixed spacing of 0.5 mm was used between indentations.

Figure 3.10. depicts the highest hardness values for the three $Al_xCoFeNiCu_{1-x}$ (x = 0.25, 0.5, 0.75) high entropy alloys that were observed around the top regions of the deposits. The maximum hardness values of $Al_xCoFeNiCu_{1-x}$ (x = 0.25, 0.5, 0.75) alloys were 462 HV, 603.4 HV and 634.3 HV, respectively.

According to these results, the deposits of $Al_xCoFeNiCu_{1-x}$ (x = 0.25, 0.5, 0.75) alloys have an average hardness of 426.3 HV, 519.4 HV, and 541.1 HV, respectively, and these values are much higher than the hardness values of the substrate SS304. This occurrence can be attributed to the effect of rapid cooling during the LMD process. This causes finer microstructure and results in excellent material properties. In addition, due to the differences in elements' atomic radii, the resultant lattice distortion causes the solid-solution strengthening effect [20,25].

With the increase of the Al content and the decrease of the Cu content, the hardness values of $Al_xCoFeNiCu_{1-x}$ (x = 0.25, 0.5, 0.75) were observed to increase. According to the XRD results, $Al_{0.25}CoFeNiCu_{0.75}$ and $Al_{0.5}CoFeNiCu_{0.5}$ had a predominantly FCC structure, while $Al_{0.75}CoFeNiCu_{0.25}$ had a combined FCC + BCC structure. With the increase of Al content, the increased BCC structure is expected to enhance the hardness of the alloys. Higher values of hardness correlate with higher strengths and wear resistance.

In comparison to the SS304 substrate, all compositions show larger hardness. Therefore, the current alloy system has the potential application for wear resistant coatings.

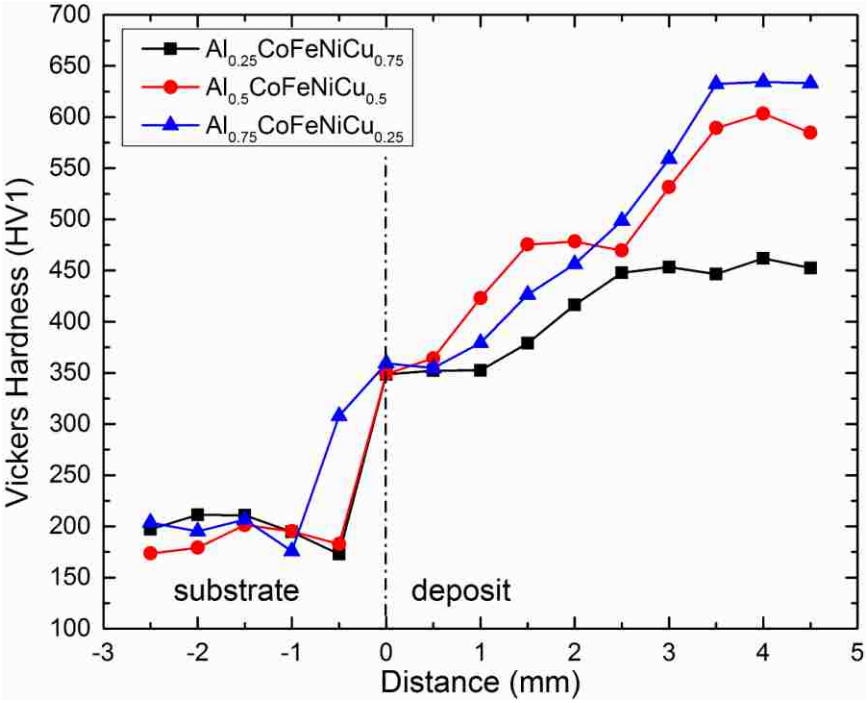

Figure 3.10. The Vickers Hardness results of the $Al_xCoFeNiCu_{1-x}$ (x = 0.25, 0.5, 0.75) alloys

4. CONCLUSIONS

The current research was implemented to investigate the feasibility of fabricating high entropy alloys of the material system $Al_xCoFeNiCu_{1-x}$ (x = 0.25, 0.5, 0.75) via the LMD process. The fabricated material was characterized using techniques such as optical microscopy, electron microscopy, hardness testing, EDS, EBSD, and XRD. The conclusions from the analyses include:

- $Al_xCoFeNiCu_{1-x}$ (x = 0.25, 0.5, 0.75) high entropy alloys have been successfully fabricated by the LMD technique using blended Al-Co-Fe-Ni-Cu elemental powder as the feedstock.
- XRD analysis revealed $Al_{0.25}CoFeNiCu_{0.75}$ and $Al_{0.5}CoFeNiCu_{0.5}$ to have the FCC lattice structure, while $Al_{0.75}CoFeNiCu_{0.25}$ was composed of both FCC and BCC lattice structure. The lattice parameters of $Al_xCoFeNiCu_{1-x}$ (x = 0.25, 0.5, 0.75) alloys were calculated and tabulated, and the increasing Al content resulted in an increase in lattice parameters of FCC structure.
- $Al_xCoFeNiCu_{1-x}$ (x = 0.25, 0.5, 0.75) fabrications contained columnar dendritic microstructure;
- Results from EBSD analysis validated that $Al_{0.25}CoFeNiCu_{0.75}$ and $Al_{0.5}CoFeNiCu_{0.5}$ were predominantly FCC in structure, and $Al_{0.75}CoFeNiCu_{0.25}$ was constituted of FCC and BCC lattice structure.
- EDS elemental maps of $Al_xCoFeNiCu_{1-x}$ (x = 0.25, 0.5, 0.75) fabrications showed the dendritic phase was Fe and Co enriched, whereas the matrix was Cu and Al enriched.
- $Al_xCoFeNiCu_{1-x}$ (x = 0.25, 0.5, 0.75) alloys had an average Vickers hardness of 426.3 HV, 519.4 HV and 541.1 HV, respectively. With the increase of Al content, a higher hardness was observed. Large amounts of Al are expected to cause severe lattice distortion, and this is expected to strengthen the solid solution and result in the high values of hardness.
- The high hardness prompts a potential application in wear resistant coatings.

ACKNOWLEDGMENT

The authors would like to thank the support from NSF (National Science Foundation) grants CMMI-1547042 (Civil, Mechanical and Manufacturing Innovation) and CMMI-1625736. The support from the Intelligent Systems Center (ISC) and Material Research Center (MRC) for the help in sample preparation and test is also appreciated.

AUTHOR CONTRIBUTIONS

For this research article, Xueyang Chen designed and performed the experiments, and analyzed the data and wrote the manuscript; Lei Yan assisted in revising figures; Sreekar Karnati assisted in paper review; Yunlu Zhang assisted in SEM analysis, and Frank Liou guided the direction of the research.

REFERENCES

[1] Katakam, S.; Joshi, S.S.; Mridha, S.; Mukherjee, S.; Dahotrea, N.B. Laser assisted high entropy alloy coating on aluminum Microstructural evolution. *J. Appl. Phys.* **2014**, *116*, 104906.

[2] Zhang, H.; Pan, Y.; He, Y.-Z. Synthesis and characterization of FeCoNiCrCu high-entropy alloy coating by laser cladding. *Mater. Des.* **2011**, *32*, 1910–1915.

[3] Zhang, S.; Wu, C.L.; Yi, J.Z.; Zhang, C.H. Synthesis and characterization of FeCoCrAlCu high-entropy alloy coating by laser surface alloying. *Surf. Coat. Technol.* **2015**, *262*, 64–69.

[4] Zhang, H.; Pana, Y.; He, Y.; Jiao, H. Microstructure and properties of 6FeNiCoSiCrAlTi high-entropy alloy coating prepared by laser cladding. *Appl. Surf. Sci.* **2011**, *257*, 2259–2263.

[5] Qiu, X.-W. Microstructure and properties of AlCrFeNiCoCu high entropy alloy prepared by powder metallurgy. *J. Alloys Compd.* **2013**, *555*, 246–249.

[6] Wang, W.-R.; Wang, W.-L.; Yeh, J.-W. Phases, microstructure and mechanical properties of Al_xCoCrFeNi high-entropy alloys at elevated temperatures. *J. Alloys Compd.* **2014**, *589*, 143–152.

[7] Tong, C.-J.; Chen, Y.-L.; Yeh, J.-W.; Lin, S.-J.; Chen, S.-K.; Shun, T.-T.; Tsau, C.-H.; Chang, S.-Y. Microstructure characterization of Al_xCoCrCuFeNi high-entropy alloy system with multiprincipal elements. *Metall. Mater. Trans.* **2005**, *36*, 881–893.

[8] Wang, W.-R.; Wang, W.-L.; Wang, S.-C.; Tsai, Y.-C.; Lai, C.-H.; Yeh, J.-W. Effects of Al addition on the microstructure and mechanical property of Al_xCoCrFeNi high-entropy alloys. *Intermetallics* **2012**, *26*, 44–51.

[9] Yang, T.; Xia, S.; Liu, S.; Wang, C.; Liu, S.; Zhang, Y.; Xue, J.; Yan, S.; Wang, Y. Effects of AL addition on microstructure and mechanical properties of Al_xCoCrFeNi High-entropy alloy. *Mater. Sci. Eng. A* **2015**, *648*, 15–22.

[10] Wang, X.F.; Zhang, Y.; Qiao, Y.; Chen, G.L. Novel microstructure and properties of multicomponent CoCrCuFeNiTi_x alloys. *Intermetallics* **2007**, *15*, 357–362.

[11] Chen, S.Y.; Yang, X.; Dahmen, K.A.; Liaw, P.K.; Zhang, Y. Microstructures and Crackling Noise of Al_xNbTiMoV High Entropy Alloys. *Entropy* **2014**, *16*, 870–884.

[12] Stepanov, N.D.; Shaysultanov, D.G.; Salishchev, G.A.; Tikhonovsky, M.A.; Oleynik, E.E.; Tortika, A.S.; Senkov, O.N. Effect of V content on microstructure and mechanical properties of the CoCrFeMnNiV_x high entropy alloys. *J. Alloys Compd.* **2015**, *628*, 170–185.

[13] Chuna, C.K.; Leong, K.F.; Lim, C.S. *Rapid Prototyping: Principles and Applications*, 2nd ed.; World Scientific: Singapore, Singapore, 2003.

[14] Unocic, R.R.; DuPont, J.N. Composition control in the direct laser deposition process. *Metall. Mater. Trans.* **2003**, *34*, 439–445.

[15] Gedda, H.; Kaplan, A.; Powell, J. Melt-solid interactions in laser cladding and laser casting. *Metall. Mater. Trans.* **2005**, *36*, 683–689.

[16] Yan, L.; Chen, X.; Li, W.; Newkirk, J.; Liou, F. Direct laser deposition of Ti-6Al-4V from elemental powder blends. *Rapid Prototyp. J.* **2016**, *22*, 810–816.

[17] Zhang, Y.; Zhou, Y.J.; Lin, J.P.; Chen, G.L.; Liaw, P.K. Solid-Solution Phase Formation Rules for Multi-component Alloys. *Adv. Mater. Eng.* **2008**, *10*, 534–538.

[18] Yang, X.; Zhang, Y. Prediction of high-entropy stabilized solid-solution in multi-component alloys. *Mater. Chem. Phys.* **2012**, *132*, 233–238.

[19] Fang, S.S.; Xiao, X.S.; Xia, L.; Li, W.H.; Dong, Y.D. Relationship between the widths of supercooled liquid regions and bond parameters of Mg-based bulk metallic glasses. *J. Non-Cryst. Solids* **2003**, *321*, 120–125.

[20] Takeuchi, A.; Inoue, A. Quantitative evaluation of critical cooling rate for metallic glasses. *Mater. Sci. Eng.* **2001**, *304*, 446–451.

[21] Kittel, C. *Introduction to Solid State Physics*, 8th ed.; John Wiley & Sons, Inc.: Hoboken, NJ, USA, 2004.

[22] Takeuchi, A.; Inoue, A. Classification of Bulk Metallic Glasses by Atomic Size Difference, Heat of Mixing and Period of Constituent Elements and Its Application to Characterization of the Main Alloying Element. *Mater. Trans.* **2005**, *46*, 2817–2829.

[23] Wang, Y.P.; Li, B.S.; Ren, M.X.; Yang, C.; Fu, H.Z. Microstructure and compressive properties of AlCrFeCoNi high entropy alloy. *Mater. Sci. Eng. A* **2008**, *491*, 154–158.

[24] Tung, C.-C.; Yeh, J.-W.; Shun, T.-T.; Chen, S.-K.; Huang, Y.-S.; Chen, H.-C. On the elemental effect of AlCoCrCuFeNi high-entropy alloy system. *Mater. Lett.* **2007**, *61*, 1–5.

[25] Hsu, U.S.; Hung, U.D.; Yeh, J.W.; Chen, S.K.; Huang, Y.S.; Yang, C.C. Alloying behavior of iron, gold and silver in AlCoCrCuNi-based equimolar high-entropy alloys. *Mater. Sci. Eng. A* **2007**, *92*, 403–408.

IV. DESIGN AND FABRICATION OF FUNCTIONALLY GRADED MATERIAL FROM TI TO Γ-TIAL BY LASER METAL DEPOSITION

Xueyang Chen[1], Lei Yan[1], Joe Newkirk[2], and Frank Liou[1]

[1]Department of Mechanical and Aerospace Engineering,

[2]Department of Materials Science and Engineering,

Missouri University of Science and Technology, Rolla, MO 65409

ABSTRACT

Functionally graded material (FGM) is one kind of advanced material characterized by a gradual change in properties as the position varies. The spatial variation of compositional and microstructure over volume is aimed to control corresponding functional properties. In this research, when 100% γ-TiAl was directly deposited on pure Ti substrate, cracks were formed within the γ-TiAl layer. Then a six-layer crack-free functionally graded material of Ti/TiAl was designed and fabricated by laser metal deposition (LMD) method, with composition changing from pure Ti on one side to 100% γ-TiAl on the other side. The fabricated FGM was characterized for material properties by a variety of techniques. The chemical compositions, microstructure, phases, and hardness of the composite were characterized by Scanning Electronic Microscope (SEM), Optical Microscope (OM), Energy Dispersive X-ray Spectroscopy (EDS), and hardness testing. The microstructure and chemical compositions in different layers were studied.

Keywords: Functionally graded material; Elemental powder; γ-TiAl; Laser metal deposition

1. INTRODUCTION

The origin of functionally graded material (FGM) is from the National Aerospace Laboratory of Japan in 1984 during a spaceplane project. The proposed thermal barrier material is capable of withstanding a surface temperature of 2000 K and a temperature gradient of 1000 K across a 10 mm section [1]. FGM is one kind of advanced material characterized by a gradual change in properties as the position varies. The spatial variation of compositional and microstructure over volume is aimed at controlling corresponding functional properties, such as mechanical properties, thermal properties, electrical properties, etc. In FGM research, various methods to prepare and fabricate FGM materials are available. The fabrication methods include powder metallurgy [2], [3], thermal spraying [4] [5], additive manufacturing [6], [7]. Additive manufacturing is a manufacturing method that can create 3D objects. This method allows you to produce complex products with minimal lead times directly from the 3D CAD models by adding layers of materials on top of each other. The bind layers schematic could mix elemental powders of variable ratios in separate layers to fabricate FGM parts with controllable gradients, no matter the complexity [8].

There is a wide range of applications for FGM and different types of FGMs could be used in different areas of application. In aerospace and automotive area, the space shuttle utilized the FGM material made of ceramic and metal that can provide the thermal protection and load carrying capability to replace the ceramic tiles that easily to crack [9]. FGMs are also used as dental implants in the biomedical area [10], vehicle armor in defense area [11], high-density magnetic recording media in optical applications [9], cutting tools in the industry [12] etc.

Actually, compressors and turbine disks are two of the most significant parts in the aerospace industry. Turbine disks require different material properties at different regions. The rim region suffers from high temperature, requires good oxidation resistance. The core region has a relatively low temperature but requires high strength. The rim and the core have different requirements. The current approach is to use different treated nickel-based superalloys for each part. Nickel-based alloys are widely used in jet engines because it could withstand high-temperatures. In aerospace applications, Ti has a combination of excellent properties but has limitation for oxidation resistance. While, intermetallic titanium alloys such as γ-TiAl, Ti_3Al can have higher oxidation resistance and both of the two alloys can be used under high temperature. Because the density for the γ-TiAl is much lower than the nickel-based superalloys and its specific properties, γ-TiAl tends to replace them. In this way, the rim can be made of Ti_3Al or γ-TiAl, which have good high-temperature properties. And the core can be made of Ti with good strength at relatively low temperatures. However, there are some problems to join them effectively. Thus, the aim of this project is to manufacture Ti/γ-TiAl functionally gradient material (FGM) using Laser Metal Deposition (LMD) method. LMD is one of the advanced additive manufacturing technologies. It could fabricate complex near net shape metallic parts layer by layer directly from computer-aided design (CAD) models. This technique could reduce cost by reducing the buy-to-fly ratio and lead time of production.

The main goals of this work involved studying the microstructure and mechanical properties of the fabricated alloys. In this study, commercially purified (CP) titanium plate was used as the substrate material for all the depositions. The powder material was fabricated as thin wall depositions and characterized for material properties using optical

and Scanning Electron Microscope (SEM) microstructure characterization, hardness testing, Energy Dispersive X-ray Spectroscopy (EDS). The study investigated the material properties of γ-TiAl manufactured by LMD method. And it showed the possibility to control properties and crack formation in the deposits. Also, it demonstrated the approach to build a complex FGM system (Ti + γ-TiAl and/or any intermediate FGM materials in between) by LMD method with hope to move to more exotic material compositions in the future.

2. MATERIALS AND METHODS

2.1. MATERIAL PREPARATION

Under the current study, commercially purified gas atomized γ-TiAl (Ti-48Al-2Cr-2Nb) powder and pure Ti powder were used as precursor materials. For this kind of γ-TiAl powder, the addition of Cr element can increase the ductility of the material. The addition of Nb element is to enhance the oxidation resistance. Blends of the two kinds of powder with different composition were made to achieve layers in functionally graded materials (FGM). The particle size distributions of γ-TiAl and Ti powder are listed in Table 2.1. and Table 2.2. individually. The chemical compositions of the two kinds of powder are given in Table 2.3. and Table 2.4. Commercially purified (CP) titanium plate was used as the substrate material for these depositions, and substrates were prepared to the dimensions of 2 × 0.5 × 0.25 in.

Table 2.1. Particle size distribution of Ti-48Al-2Cr-2Nb powder (% Under)

Particle Size (μm)	150	106	75	63	53	Apparent Density (g/cc)
By Mass	99.9	66.2	25.5	14.7	4.0	2.20

Table 2.2. Particle size distribution of Ti powder (% Under)

Particle Size (μm)	150	53	Apparent Density (g/cc)
By Mass	98.9	0.9	2.64

Table 2.3. Chemical analysis of Ti-48Al-2Cr-2Nb powder (wt.%).

Elements	Ti	Al	Cr	Nb	Fe	Si	C	O
Measured	Balance	34.4	2.38	4.75	0.04	0.016	0.014	0.128

Table 2.4. Chemical analysis of Ti powder (wt.%).

Elements	Ti	C	O	N	H	Fe	Other
Measured	Balance	<0.01	<0.16	<0.01	<0.001	<0.12	<0.4

2.2. DEPOSITION SYSTEM

In this study, a 1 kW continuous wave fiber laser with a wavelength of 1064 nm was used to deposit the elemental powder blends. A melt pool spot size of approximately 2 mm was obtained through a lens of 750 mm focal length. A ceramic tube nozzle was used in conjuncture with a CNC (Computer Numerical Control) table to facilitate movement

and perform deposition. Argon gas was used to implement an inert atmosphere and was also used as a carrier gas to deliver the powder mixture to the melt pool.

The schematic layout of the LMD system is shown in Figure 2.1. LMD deposition is an additive manufacturing technique capable of fabricating complicated structures with superior properties [13]. The applications of this technique include coatings, rapid prototyping, tooling, repair, etc. LMD uses a focused laser beam as a heat source to create a melt pool into which powder feedstock is injected. The powder material is metallurgically bonded to the substrate through solidification [14].

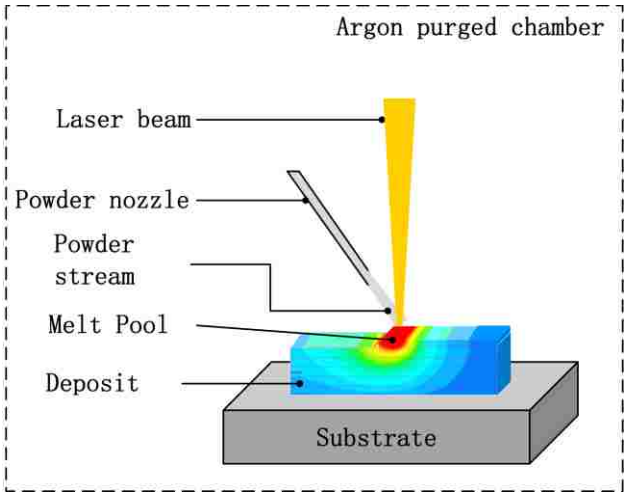

Figure 2.1. Schematic layout of the LMD (Laser Metal Deposition) system [15]

2.3. EXPERIMENTAL PROCEDURE

In this research, three kinds of experiments have been designed in order to get crack-free Ti/γ-TiAl deposit.

In the first kind of experiment, set-up 1 has been used to deposit Ti-48Al-2Cr-2Nb powder on CP Ti substrate directly, as Figure 2.2. (a) showed below.

In this set-up, the substrates were directly connected with the fixture. Thin wall depositions were fabricated by performing single melt pool layer by layer. Before deposition, a preheat scan of running the laser across the substrate surface at 1 kW power without powder was performed, in order to ensure perfect bonding. The preheating process was also used to heat up the substrate and rid the surface of the substrate from oxide scale buildup, surface impurities, and, surface imperfections. Laser transverse speed was set at 600 mm/min for all the depositions. The laser power was set at 600 W. The initial 2 layers of deposition carried out a duty cycle of 100% to ensure perfect bonding with the substrate. The next 4 layers keep the duty cycle of 80% and then drop to 60% for another 4 layers. The rest of the deposition was carried at a duty cycle of 40%. The actual laser power is calculated by multiplying the laser power by the duty cycle. The same deposition scheme and parameters were used for all the depositions. This was expected to ensure an unbiased comparison between different depositions.

The second kind of experimental design used the set-up 2 as shown in Figure 2.2. (b). The insulating refractory bricks were inserted between the substrate and the fixture.

The third experimental design was used to manufacture the crack-free functionally gradient material (FGM) from Ti to γ-TiAl. The FGM study included material design, material preparation, and evaluation of material properties. The FGM path was developed as shown in Figure 2.3. The atomic percentage of each element and possible phase composition of every layer in the FGM deposit are also listed in Table 2.5.

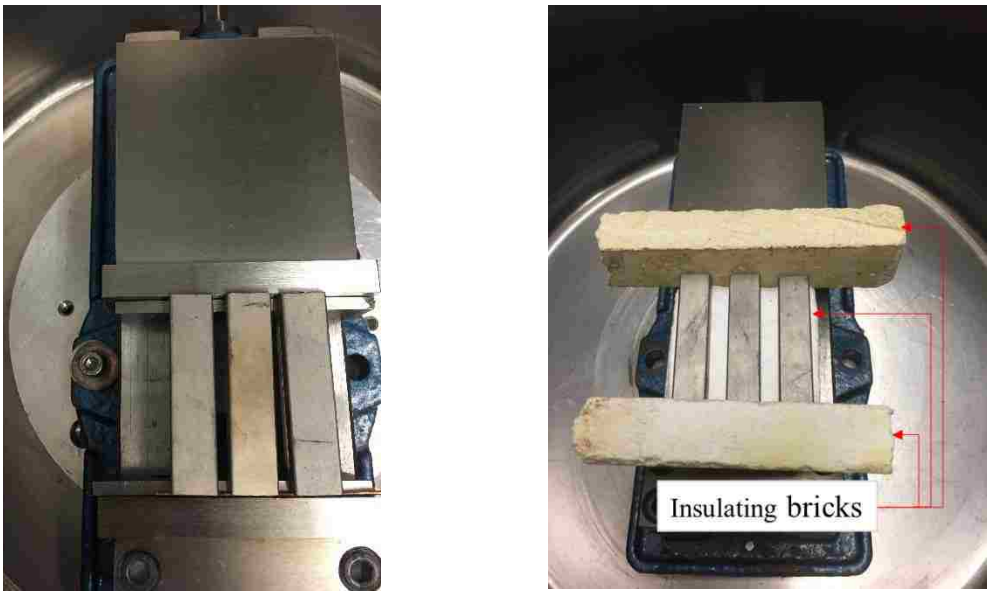

(a) (b)

Figure 2.2. Two experimental set-ups. (**a**) Set-up 1; (**b**) Set-up 2.

Powders were weighed for desired compositions in a glove box under an argon atmosphere and sealed in bottles before starting the deposition process. In this study, γ-TiAl powder and pure Ti powder were used. The as-blended powder mixtures can be used to form the layers in the functionally graded materials. These bottles were then shaken using a Turbula® mixer (Glen Mills Inc., Maywood, NJ, United States) for 20 min to obtain thorough mixing and homogeneity within the powder blends. During the process, there is no insulating brick used here by taking use of the first experimental set-up (set-up 1).

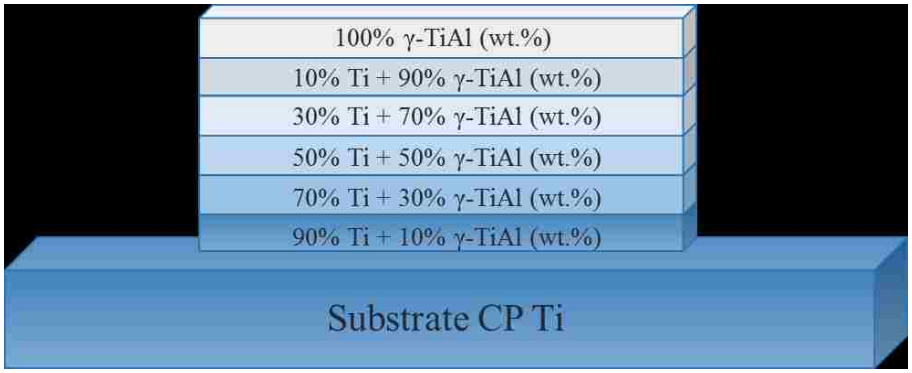

Figure 2.3. The designed functionally graded material (FGM) path.

Table 2.5. Particle size distribution of Ti-48Al-2Cr-2Nb powder (% Under).

Weight Percentage	**Ti at.%**	**Al at.%**	**Cr/Nb at.%**	**Possible Phase Composition**
100% γ-TiAl	48.00	48.00	2.00	$\alpha_2 + \gamma$
10% Ti + 90% γ-TiAl	52.30	44.03	1.83	$\alpha_2 + \gamma$
30% Ti + 70% γ-TiAl	61.40	35.63	1.48	$\alpha_2 + \gamma$
50% Ti + 50% γ-TiAl	71.28	26.51	1.10	α_2
70% Ti + 30% γ-TiAl	82.01	16.60	0.69	$\alpha_2 + \alpha$
90% Ti + 10% γ-TiAl	93.73	5.79	0.24	α

After deposition, vertical transverse sections were cut using a wire Electro-Discharge Machine (wire-EDM, Hansvedt Industries Inc., Rantoul, IL, United States) and mounted in Bakelite for grinding and polishing. Kroll's reagent containing 30 ml H_20, 10ml HNO_3, and 10 ml HF was used for etching the samples. Hirox optical microscope was used to perform microstructure imaging. Helios Nanolab 600 SEM (FEI Company, Hillsboro, OR, United States) equipped with an Oxford Energy Dispersive Spectrometer was used to get the chemical compositions. The Vickers hardness measurements were performed using

a Struers Duramin micro-hardness tester (Struers Inc., Cleveland, OH, United States). Press load of 9.81 N and load time of 10 s was used during the hardness tests.

3. RESULTS AND DISCUSSION

3.1. DEPOSIT PROFILE

Figure 3.1. shows the deposited samples in the first experimental design. The image of the γ-TiAl deposit made by using set-up 1 in the first design has been shown in Figure 3.1. (a). It could be seen that there are some cracks in the deposit. Then with the same setup, another deposited sample was made from the powder blend of 80 wt.% γ-TiAl +20 wt.% Ti. Figure 3.1.(b) demonstrates the 80 wt.% γ-TiAl +20 wt.% Ti sample deposited by using set-up 1. It has been found that it is possible to make crack-free deposits with the blend. It is theorized that the cracks that mainly exist in the vertical direction are caused by residual stress. It is known that there exists a great difference in the thermal expansion coefficient between Ti and γ-TiAl. Ti has the thermal expansion coefficient of $8.9 \times 10^{-6}K^{-1}$, while γ-TiAl shows $14.4 \times 10^{-6}K^{-1}$. Due to the high residual thermal stresses between the Ti and γ-TiAl layers, it would result cracks during the cooling process after deposition. However, the layer of Ti + γ-TiAl deposits could play a role in reducing the interfacial residual thermal stresses. Therefore it could cause some cracks in the deposit by directly depositing γ-TiAl powder on Ti substrate, however crack-free γ-TiAl deposit could be made on the Ti substrate by using the powder blend of γ-TiAl and 20 wt.% Ti.

(a) (b)

Figure 3.1. Deposited samples in the first experimental design. (a) γ-TiAl sample without insulating bricks; (b) 80 wt.% γ-TiAl +20 wt.% Ti sample without insulating bricks

Then in order to get a crack-free γ-TiAl deposit, the set-up 2 has been used in the second experimental design, as shown in Figure 2.2. (b). The image of the γ-TiAl deposit made by using set-up 2 has been shown in Figure 3.2. It has been found that the deposited sample has no cracks. In this set-up, the insulating bricks were inserted between the substrate and the fixture. Because these materials thermally isolate the substrate, the bricks could retain more of the input laser energy and decrease cooling rate. Then many conditions, such as boundary conditions, thermal insulation, and post-process heat treatment, may affect the mechanical properties of deposits.

Figure 3.2. Deposited sample in the second experimental design

However, it is not very flexible to fabricate some big and complex parts with insulating bricks in the industry area. It is necessary to develop a gradient path to realize the same target of depositing crack-free γ-TiAl deposit on Ti substrate. Then an FGM path has been designed, as shown in Figure 2.3. The objective of the designed FGM is to meet the expected requirements by eliminating the obvious interface between composite materials in different layers, just the same as bones, teeth, etc. in nature. Also, the FGM is also designed to accommodate materials for specific applications. During the FGM deposition process, there was no insulating brick used. From Figure 2.3., the FGM parts were made with five different powder blends and the top layer is 100% γ-TiAl. Along the deposit, there are six regions with different chemical composition. The gradients between different layers could smooth transition to reduce the opportunity of failure. The transient layer of Ti + γ-TiAl deposits could gradually reduce the residual thermal stresses. Figure 3.3. showed the image of the FGM deposit and its transverse section after cutting.

(a) (b)

Figure 3.3. Deposited sample in the FGM design. (a) FGM sample; (b) Transverse section of the FGM deposit

3.2. VICKERS HARDNESS

Figure 3.4. shows the Vickers hardness distribution of the deposited samples without using insulating bricks in the first experimental design. By applying post heat treatment during the deposition process, the Vickers hardness values of the deposits could also be compared in this Figure. It was observed that the Vickers hardness values of the γ-TiAl layers varied around 375 HV in the middle part of the deposit zone, then increased to 450 HV as it progressed into the top of the deposit. While the deposit by using the powder blends of 80 wt.% γ-TiAl +20 wt.% Ti had a Vickers hardness of around 420 HV. The literature reported γ-TiAl Vickers hardness was 425 HV. And when comparing the two kinds of deposits under different conditions of performing post heat treatment or not, it has been found that the post heat treatment on deposit would increase the hardness values, but could not make significant changes.

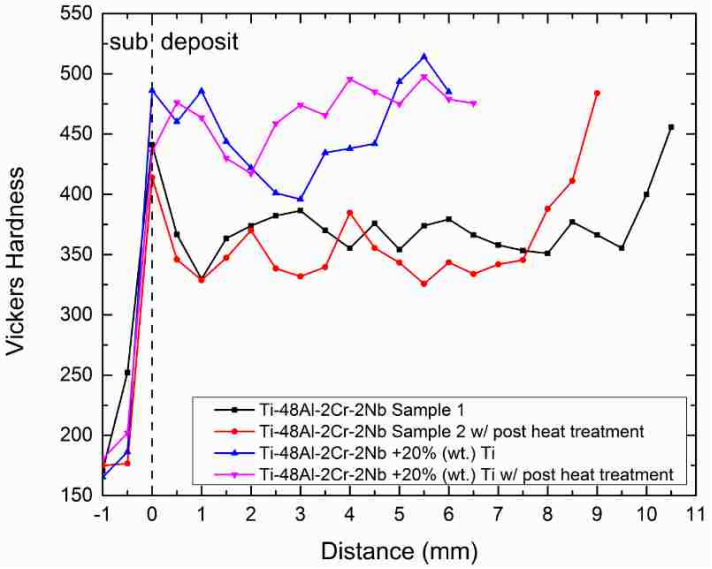

Figure 3.4. Vickers hardness distribution of the deposited samples in the first experimental design

Figure 3.5. shows the hardness distribution of the deposited samples under different laser power with using insulating bricks in the second experimental design. It can be observed that when other parameters stayed the same, the higher the laser power, the lower the Vickers hardness. The reason should be the increase of the energy input. It would decrease the cooling rate, and then cause coarser microstructure and get lower hardness values. Therefore with insulating bricks to decrease the cooling rate, it is much easier to get crack-free γ-TiAl deposits.

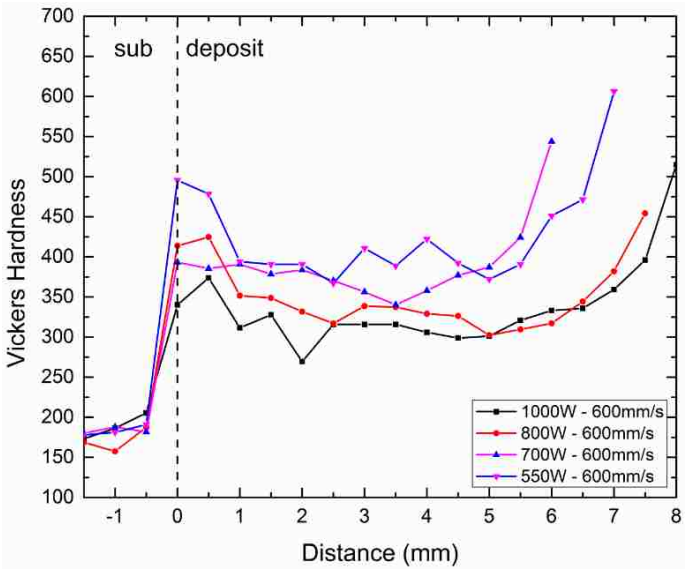

Figure 3.5. Vickers hardness distribution of the deposited samples in the second experimental design

In this research, three kinds of experiments have been designed in order to get crack-free Ti/γ-TiAl deposit.

Functionally graded materials (FGM) is one kind of advanced material. They have a gradual change in properties as the position varies. As shown in this Figure 2.3., the volume fraction of one material will change from 100% on one side to zero on another side, and another constituent will change in the other way around. Their composition and microstructure vary in space by following a predetermined law. This change also leads to a gradient of properties and performance, such as mechanical properties, thermal properties. Figure 3.6. shows the Vickers hardness distribution of the FGM sample. The 100% γ-TiAl layer is harder than previous composition layers.

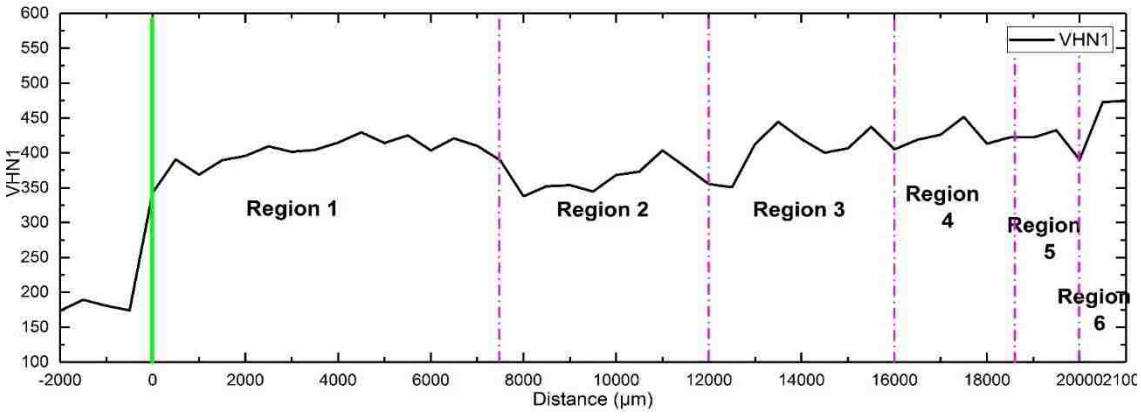

Figure 3.6. Vickers hardness distribution of the FGM sample

3.3. MICROSTRUCTURE & EDS TEST

The microstructures of γ-TiAl deposits from Set-up 1 and Set-up 2 are shown in Figure 3.7. It shows that most prevalent microstructure for both is lamellar.

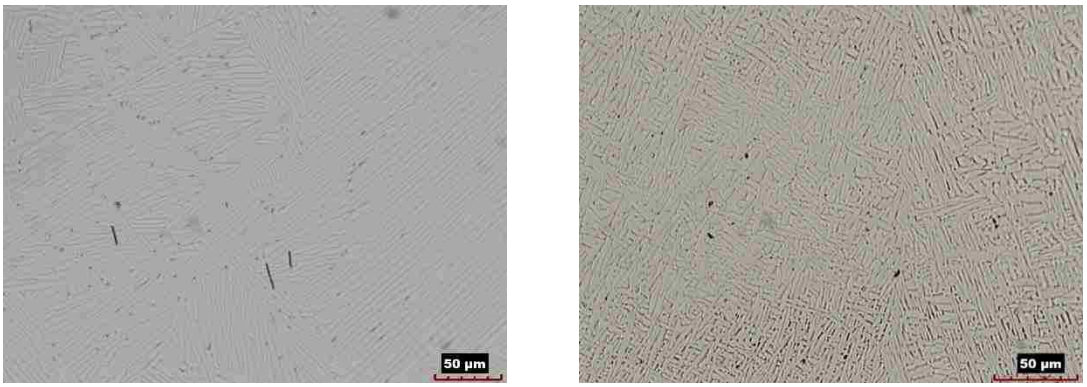

(a) (b)

Figure 3.7. Microstructures of the γ-TiAl from two set-ups. (**a**) Microstructure of the γ-TiAl from set-up 1; (**b**) Microstructure of the γ-TiAl from set-up 2

Figure 3.8. shows the EDS result of the FGM deposit. Line scan was performed along the deposit, it differentiated six regions with different compositions listed in Table 2.5. The designed length for each region is 5 mm. Region height difference can be attributed to the powder capture efficiency.

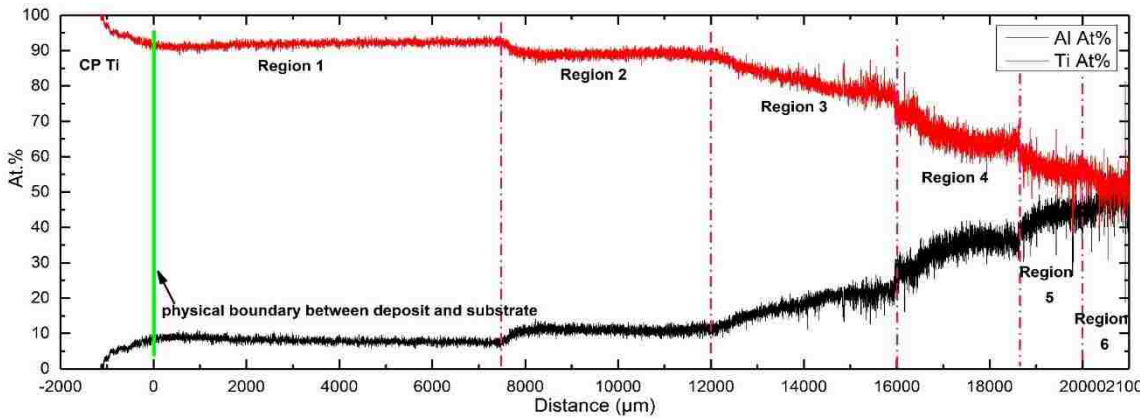

Figure 3.8. EDS result of the FGM deposit

4. CONCLUSIONS

The current research was implemented to investigate the feasibility of combining Ti with γ-TiAl via the LMD process. The fabricated material was characterized using techniques such as scanning electron microscopy, hardness testing, EDS. The conclusions from the analyses include:

- Crack-free γ-TiAl deposits could be fabricated by using insulating bricks to control the cooling rate during LMD process.
- Proposed an FGM path to successfully join titanium alloy with γ-TiAl.
- Mechanical properties of γ-TiAl would be affected by are affected by processing parameter. Increasing energy input would decrease the cooling rate and decrease the Vickers hardness.

The microstructure in the γ-TiAl deposit is lamella.

ACKNOWLEDGMENT

This project was supported by The Boeing Company through the Center for Aerospace Manufacturing Technologies (CAMT). Their financial support is greatly appreciated.

REFERENCES

[1] M. KOIZUMI, "FGM ACTIVITIES IN JAPAN," *Compos Part B Eng*, vol. 28, pp. 1–4, 1997.

[2] a. Shahrjerdi, F. Mustapha, M. Bayat, S. M. Sapuan, and D. L. a. Majid, "Fabrication of functionally graded Hydroxyapatite- Titanium by applying optimal sintering procedure and powder metallurgy," *Int. J. Phys. Sci.*, vol. 6, no. 9, pp. 2258–2267, 2011.

[3] F. Thummler and R. Oberacker, *Introduction to Powder Metallurgy*, vol. 34, no. 3. 1995.

[4] V. Cannillo, L. Lusvarghi, T. Manfredini, M. Montorsi, C. Siligardi, and A. Sola, "Glass-ceramic functionally graded materials produced with different methods," *J. Eur. Ceram. Soc.*, vol. 27, no. 2–3, pp. 1293–1298, 2007.

[5] M. Belmonte, J. Gonzalez-Julian, P. Miranzo, and M. I. Osendi, "Continuous in situ functionally graded silicon nitride materials," *Acta Mater.*, vol. 57, no. 9, pp. 2607–2612, 2009.

[6] T. Durejko, M. Zietala, W. Polkowski, and T. Czujko, "Thin wall tubes with Fe3Al/SS316L graded structure obtained by using laser engineered net shaping technology," *Mater. Des.*, vol. 63, pp. 766–774, 2014.

[7] H. S. Ren, X. J. Tian, and H. M. Wang, "Effect of heat treatment on microstructure and mechanical properties of a graded structural material," *Mater. Sci. Eng. A*, vol. 614, pp. 207–213, 2014.

[8] M. S. El-Wazery and A. R. El-Desouky, "A review on functionally graded ceramic-metal materials," *J. Mater. Environ. Sci.*, vol. 6, no. 5, pp. 1369–1376, 2015.

[9] A. Saiyathibrahim, S. S. Mohamed Nazirudeen, and P. Dhanapal, "Processing Techniques of Functionally Graded Materials - A Review," *Proc. Int. Conf. Syst. Sci. Control. Eng. Technol.*, vol. 1, pp. 98–105, 2015.

[10] A. Tampieri, G. Celotti, S. Sprio, A. Delcogliano, and S. Franzese, "Porosity-graded hydroxyapatite ceramics to replace natural bone," *Biomaterials*, vol. 22, no. 11, pp. 1365–1370, 2001.

[11] Y. M. Soon, K. H. Shin, Y. H. Koh, J. H. Lee, W. Y. Choi, and H. E. Kim, "Fabrication and compressive strength of porous hydroxyapatite scaffolds with a functionally graded core/shell structure," *J. Eur. Ceram. Soc.*, vol. 31, no. 1–2, pp. 13–18, 2011.

[12] Y. Miyamoto, W. A. Kaysser, B. H. Rabin, A. Kawasaki, and R. G. Ford, "Functionally Graded Materials: Design, Processing and Applications," in *Kluwer Academic,* 1999.

[13] X. Chen, L. Yan, W. Li, Z. Wang, F. Liou, and J. Newkirk, "Effect of Powder Particle Size on the Fabrication of Ti-6Al-4V Using Direct Laser Metal Deposition from Elemental Powder Mixture," vol. 6, pp. 348–355, 2016.

[14] X. Chen, L. Yan, S. Karnati, Y. Zhang, and F. Liou, "Fabrication and Characterization of AlxCoFeNiCu1−x High Entropy Alloys by Laser Metal Deposition," *Coatings*, vol. 7, no. 4, 2017.

[15] X. Chen, L. Yan, W. Li, F. Liou, and J. Newkirk, "Effect of Powder Particle Size on the Fabrication of Ti-6Al-4V using Direct Laser Metal Deposition from Elemental Powder Mixture," pp. 714–722, 2016.

SECTION
2. CONCLUSION

Since most of the advanced materials are made of high-performance and high-value metals, thus the research issues on fabricating and optimizing advanced metallic components economically and efficiently. Therefore, it is very challenging and important to investigate and develop a new methodology for composition establishment, cost reduction, components fabrication and performance improvement. The elemental powder mixture has been used as feedstock in the LMD process. It offers a cost-effective possibility for near net shape fabrication. Take the fabrication of Ti-6Al-4V as an example, this alloy exhibits excellent properties, but still classified as one of the difficult-to-machine materials. Owing to the high cost of conventionally produced Ti-6Al-4V, powder processing method becomes an appealing alternative to fabricate the titanium alloy for cost reduction. In this case, industry qualified Ti-6Al-4V components can be produced by using Ti, Al and V powder mixture and these elemental powders have close particle number in the mixture. Each individual advanced metallic component could be unique, the required composition is specific and arbitrary. Since it always has a problem to get target material with the original designated ratio for the elemental powders due to powder separation, the principle of the powder motion is researched. It reveals that the particle number for each element in the powder mixture is a key factor for composition control in the deposit components.

In order to extend the application of the elemental approach to a broader area for the LMD process, the fabrication of AlxCoFeNiCu1−x (x = 0.25, 0.5, 0.75) high entropy alloys are proposed. High entropy alloys are novel material systems that exhibit properties much more superior than traditional alloys. In this research, the material system

AlxCoFeNiCu1−x (x = 0.25, 0.5, 0.75) have been fabricated using blended Al-Co-Fe-Ni-Cu elemental powder as the feedstock. Analyzing the deposit parts using optical microscopy, electron microscopy, EDS, EBSD, XRD and hardness testing techniques reveals the properties of the alloys. The experimental results show that the method is more flexible and feasible for novel metallic materials development with elemental powder mixture.

Moreover, the research and application of elemental approach on functionally gradient materials (FGM) are developed. Because FGM is one kind of advanced material characterized by a gradual change in properties as the position varies, it is more controllable to form transition layers by blending various elemental powders to eliminate the obvious interface and accommodate gradients for specific applications. Also, the LMD manufacturing method allows producing such complex components with minimal lead time by directly adding materials layer by layer from 3D CAD models. The overall goal for this process planning is to propose an FGM path to join titanium alloy with γ-TiAl without cracks along the build. In addition, the process also provides a series of technical approaches for analyzing the properties of the materials. Compared with previous research on FGM, it dramatically simplifies the work for selecting transition materials.

The overall outcomes of this dissertation addressed several key issues which challenging the application of elemental powder mixture for advanced metallic components fabrication in LMD process. It provides the processes for developing production procedures, establishes the schema for optimizing the metallic components, generates a path, integrates the methods. The most challenging problem in the powder deposition process using LMD is to identify the strategy for each unique component. The

different trials could improve the possibility to successfully fabricate designed components with low cost. The deposited parts could be analyzed according to a series of general ways to get the mechanical properties, microstructure, phases and so on. The path pattern and deposition parameters can make a big difference for the final deposited parts. There is an actual demand for the use of elemental powder to improve the economy of fabricating theory analysis for implementing the deposition. The proposed experiment plan and analysis method will be applied to fabricate different types of complex components from different areas. The powder deposition process and the generation method for the FGM transition path could be extended to fabricate other new types of materials to improve the components' properties and reduce cost. Many complex parts are also feasible by adding secondary operations such as machining to complete the shape of the deposited part, and by following certain design path. The potential application of developed alloys could tell the feasibility to develop new materials and improve the efficiency to research new area by using a blended elemental powder mixture.

BIBLIOGRAPHY

[1] J. W. Adams, V. A. Duz, V. S. Moxson, and W. R. Roy, “Low Cost Blended Elemental Titanium Powder Metallurgy,” no. Mmc, 1890.

[2] M. Qian and F. H. Sam Froes, *Titanium powder metallurgy: Science, technology and applications*. 2015.

[3] S. Katakam, S. S. Joshi, S. Mridha, S. Mukherjee, and N. B. Dahotre, “Laser assisted high entropy alloy coating on aluminum: Microstructural evolution,” *J. Appl. Phys.*, vol. 116, no. 10, pp. 0–6, 2014.

VITA

Xueyang Chen was born in Xiaochang county, Xiaogan City, Hubei province, China. She received her Bachelor of Science degree in Chemistry in July 2011 from University of Science and Technology of China, Hefei city, Anhui province, China. In December 2013, she received her Master of Science degree in Manufacturing Engineering from Missouri University of Science and Technology, Rolla, Missouri, USA. In May 2018, she received her Doctor of Philosophy in Mechanical Engineering from Missouri University of Science and Technology, Rolla, Missouri, USA. Her research interests include additive manufacturing, elemental powder manufacturing, and laser deposition. During her Ph.D. study, she authored and co-authored seven journal papers and four conference papers.